N73-28175

NASA CONTRACTOR REPORT

NASA CR-2282

NASA CR-2282

EXPERIMENTAL AND ANALYTICAL STUDY OF ONE- AND TWO-COMPONENT FLOWS IN SPHERICAL CHAMBERS

by Bruce V. Johnson

Prepared by
UNITED AIRCRAFT RESEARCH LABORATORIES
East Hartford, Conn. 06108
for Lewis Research Center

1. Report No. NASA CR-2282	2. Government Accession No.	3. Recipient's Catalog No.
4. Title and Subtitle EXPERIMENTAL AND ANALYTICAL STUDY OF ONE- AND TWO-COMPONENT FLOWS IN SPHERICAL CHAMBERS		5. Report Date August 1973
		6. Performing Organization Code
7. Author(s) Bruce V. Johnson		8. Performing Organization Report No. UARL-M910963-36
		10. Work Unit No.
9. Performing Organization Name and Address United Aircraft Research Laboratories East Hartford, Connecticut 06108		
		11. Contract or Grant No. NAS 3-13446
		13. Type of Report and Period Covered Contractor Report
12. Sponsoring Agency Name and Address National Aeronautics and Space Administration Washington, D.C. 20546		
		14. Sponsoring Agency Code

15. Supplementary Notes

Project Manager, Henry A. Putre, Nuclear Systems Division, NASA Lewis Research Center, Cleveland, Ohio

16. Abstract

A study was conducted to evaluate techniques for obtaining high inner-gas concentrations in a spherical cavity for application to the open-cycle gaseous-core nuclear rocket. The study included flow visualization tests with water and gases as the working fluids, calculations of the streamline distribution, and calculation and measurement of the inner-gas concentration with air and Freon-11 as the inner-stream gases. The cavity shape, the outer-stream injection conditions, the turbulent transport coefficients, and the buoyancy effects were found to affect the inner-stream flow patterns.

17. Key Words (Suggested by Author(s)) Nuclear rocket; Gas core; Spherical cavity; Turbulent; Mass diffusion; Air; Freon; Concentration profiles; Containment; Fuel; Flow visualization	18. Distribution Statement Unclassified - unlimited		
19. Security Classif. (of this report) Unclassified	20. Security Classif. (of this page) Unclassified	21. No. of Pages 71	22. Price* $3.00

TABLE OF CONTENTS

SUMMARY

An experimental and analytical study was conducted to evaluate techniques for obtaining high inner-gas concentrations in a spherical cavity for application to the open-cycle gaseous-core nuclear rocket engine. The inner-stream fluid was injected into the cavity from a small diameter 'point' source to simulate vaporized nuclear fuel. The outer-stream fluid was injected through wall jets at the peripheral wall to simulate the propellant. The study was concerned with developing outer-stream injection configurations and determining outer-stream injection flow conditions that would result in good simulated-fuel containment characteristics, i.e., more than 20 percent of the cavity filled with inner-stream gas for ratios of outer-stream flow rate to inner-stream flow rate greater than 100. The study was comprised of (1) flow visualization tests conducted with water as the working fluid, (2) calculation of the streamline and inner-gas concentration contours within a cavity for several outer-stream injection conditions, fluid properties, and gravitational fields, and (3) measurement of the inner-stream concentration in a spherical cavity for tests with air as the outer-stream fluid and air and Freon-11 as the inner-stream fluids. The calculations and concentration measurement tests were carried out for a spherical cavity with a maximum diameter and length of 12 in. (30.5 cm) and 18 in. (38.1 cm), respectively, which terminated with an exhaust nozzle having a throat diameter of 2 in. (5.1 cm).

The outer stream injection component development tests, conducted in a wedge-shaped chamber, showed that the cavity peripheral wall shape, the wall-jet area distribution, the outer-stream injection distributions, and the ratio of the outer-stream flow rate to inner-stream flow rate significantly affect the inner-stream flow pattern. For the flow conditions tested, variations in the Reynolds number and use of corrugated ribbon inserts in the wall jets in the downstream section of the cavity did not affect the flow characteristics. The solution of the Navier-Stokes equations for the spherical cavity showed the complex relationship between changes in the boundary conditions or fluid properties and the streamline and inner-gas concentration contours within the cavity. Changes in the outer-stream injection flow rate per unit area, the injection angle, and the fluid viscosity had large changes in the cavity flow patterns. For concentration measurement tests in the spherical cavity with air as the inner gas, the average inner-gas partial pressure decreased from a value of 40 percent of the cavity pressure for a flow ratio equal 25 to a value of 0.15 for a flow ratio equal 100. For tests with Freon-11 as the inner gas (inner- to outer-stream density ratio equal 4.7), the average inner-gas partial pressure was 7 percent of the cavity pressure for flow ratios of 25, 50, and 100. Further development work is required to obtain desirable simulated-fuel containment in the spherical cavity with a small diameter source with ratios of simulated-fuel density to simulated-propellant density greater than one.

The goal of developing a gaseous-core nuclear rocket engine is desirable because the potential specific impulse obtainable is high (between 1500 and 5000 sec). Because of this potential, analytical and experimental studies to determine the feasibility of several open-cycle and closed-cycle versions of the gaseous-core nuclear rocket have been conducted at NASA-Lewis Research Center, the United Aircraft Research Laboratories, and elsewhere since approximately 1957. For the open-cycle gaseous-core rockets, the nuclear fuel and the propellant are both exhausted from the engine through the nozzle. For the closed-cycle gaseous nuclear rockets, the nuclear fuel is separated from the propellant by a transparent wall inside the engine and is not exhausted with the propellant. The fluid mechanics study reported herein is applicable to the open-cycle concept.

The original open-cycle coaxial-flow concept, outlined in Ref. 1, has been modified and refined such that the reactor chamber presently envisioned has an approximately spherical shape rather than the original cylindrical shape. Descriptions of the current concepts, estimates of the performance and component requirements, and a survey of previous work on open-cycle concepts are presented in Refs. 2 and 3. In all of these concepts the nuclear fuel and propellant are injected into the reactor chamber at different locations and exhausted together from the reactor chamber through the nozzle. The energy generated from nuclear fissions in the gaseous fuel is transferred to the propellant by thermal radiation. The fluid mechanics requirements are that (1) a large fraction of the reactor chamber be filled with gaseous nuclear fuel, i.e., high containment, and (2) the ratio of the propellant weight-flow rate to the gaseous nuclear fuel weight-flow rate be large.

Background Information

Coaxial Flow Studies. - Most of the previous experimental and analytical investigations of the fluid mechanics for the coaxial-flow gaseous-nuclear rocket (GNR) engine have studied coaxial jets issuing into a chamber with a sharp discontinuity between the fast moving simulated propellant in the outer stream and the slow moving simulated fuel of the inner jet. These previous studies at Lewis Research Center, Illinois Institute of Technology, and United Aircraft Research Laboratories are summarized or cited in Ref. 3. These studies were thought to be applicable to the coaxial-flow region of the engine (see Fig. 1). However, the flow which resulted from these inlet flow conditions had large or moderate scale turbulent mixing and had poor containment characteristics with respect to that required for economical operation of the rocket engine.

A flow visualization study (Ref. 4) of some of the coaxial jets described above indicated that the large eddy structure developed rapidly near the inlet plane. When these results were related to the results of previous and concurrent analytical and experimental studies of the growth of wave-like disturbances in shear layers (Refs. 5 through 7), a method of improving the containment characteristics for the coaxial-flow region was proposed (Ref. 8). This method consisted of providing a larger shear layer width at the coaxial-flow region inlet plane; the transition from the high-velocity outer stream to the lower-velocity inner jet being gradual, rather than abrupt. The flow visualization studies of Ref. 8 indicated qualitatively that a more desirable flow could be obtained with this inlet condition. The large-scale eddies found for many flow conditions in Ref. 4 were suppressed · by suitable modification of the inlet geometry. The suppression of these large-scale eddies is desirable for a full-scale reactor since this reduces mixing between fuel and propellant. The growth rate of the class of wavy disturbances observed in Ref. 8 was measured (Ref. 9) and found to agree with a companion analytical prediction for the growth of wavy disturbances in an inviscid free-shear layer with the measured velocity profile.

Concentration measurements of a two-component coaxial flow in a cylindrical cavity (Ref. 10) indicate that a simulated-fuel volume fraction of approximately 20 percent was obtained at ratios of simulated-propellant flow rate to simulated fuel flow rate greater than 200 by reducing the scale and intensity of the turbulent transport between the simulated fuel and simulated propellant to a sufficiently low level. The application of the information obtained from these and previous coaxial-flow tests at Lewis Research Center and the Illinois Institute of Technology is limited to the coaxial-flow region of the engine chamber.

Tear-Drop Cavity Studies. - Additional flow visualization studies were directed toward obtaining desirable containment flow conditions in a two-dimensional tear-drop cavity with small-diameter 'line' sources. These studies were exploratory and qualitative in that most of the effort was directed toward obtaining a desirably appearing flow rather than obtaining detailed flow measurements. The first study employing a tear-drop shaped chamber with cylindrical porous walls was conducted at Lewis Research Center (Ref. 11). This study was extended to include two-component flows in a larger cavity at Idaho Nuclear Corporation (Ref. 12).

Spherical Cavity Studies. - Since 1970, the fluid mechanics studies have been directed toward obtaining desirable containment flow conditions in an axisymmetric cavity with small diameter inner-gas sources. These studies (Refs. 12 and 14) have been exploratory and primarily qualitative in that most of the effort has been directed toward obtaining a desirable flow model rather than obtaining detailed flow measurements. During the first year of the present spherical cavity study at UARL, flow visualization studies were

conducted with air as the simulated-propellant (outer-stream) gas and Freon-11 and air as the simulated-fuel (inner-stream) gas. The qualitative results from this study (Ref. 14) showed that approximately 25 percent of the chamber could be filled with a mixture of outer stream and inner stream gases when the ratio of outer-stream flow rate to inner-stream flow rate was 100. The studies also showed that buoyancy influenced the flow for tests with Freon-11 as the inner gas and that the inner-gas containment characteristics obtained with the heavy inner gas were not suitable for the nuclear rocket.

Objectives of This Study

At present, parametric studies on the nucleonics, fluid mechanics, and heat transfer for the open-cycle reactor are being conducted or directed by the NASA Lewis Research Center. Models for each aspect of the reactor are continuously being revised, studied, and evaluated in order to provide information (e.g., Refs. 4 and 8 through 13) for parametric system studies to determine the 'tradeoffs' and feasibility of the reactor concept (Refs. 15 and 16). Therefore, the general purposes of the present study are (1) to improve the fluid mechanics characteristics in the chamber with respect to the previously mentioned fluid mechanics requirements, and (2) to provide quantitative data concerning the chamber containment characteristics.

The overall objective of the work reported herein was to experimentally obtain a large mass of simulated fuel (inner-stream fluid) in the central region of an approximately spherical cavity at the Reynolds number, weight flow ratios, and buoyancy parameters envisioned at the start of the study for use in the full-scale gaseous nuclear rocket. The approach used in working toward that objective was to conduct an outer-stream injection component development study and an analytical study calculating the flow within the spherical cavity, before designing and fabricating the spherical cavity in which the inner-gas concentration measurements and final flow visualization studies were obtained. The original objectives of the outer-stream injection component development test was to develop wall-jet configurations which would result in small-scale turbulent mixing between the outer-stream and inner-stream fluids. During the study it became apparent that the flow structure within the cavity and the tendency of the inner-stream fluid to flow toward the exhaust nozzle or to recirculate was also a strong function of the shape of the cavity wall and the ratio of the wall jet area to the wall surface area. As a result, the test program included tests to determine the effect of outer-stream injection flow conditions on the flow characteristics of constant density and two-component flows. As part of the study, the effects of buoyancy, fluid viscosity, and mass diffusivity were also investigated.

4

This flow visualization study was conducted in a wedge-shaped chamber with water as the working fluid to evaluate outer-stream injection components which would be suitable for use in the spherical cavity. Of particular concern in these tests, was the effect of the outer-stream injection geometry and flow rate distribution on the flow structure near the wall and the flow structure within the cavity. The chamber injection configuration and the flow conditions for the tests are tabulated in TABLES I and II.

Description of Test Apparatus

The outer-stream injection component development tests were conducted with the test apparatus shown in the schematic drawing of Fig. 2. Water was used as the working fluid and uranine dye was added at ten injection points for most tests as a trace fluid. Water was pumped from the reservoir tank through a manifold, variable-area flowmeters, and valves to the test chamber shown in the photographs of Fig. 3. The maximum capacity of each of the ten flowmeters was six (6) gallons per minute for a total of sixty (60) gallons per minute. This flow was obtained from a constant speed pump with a one-hundred fifty (150) gallons per minute capacity and throttled using the valve arrangement shown in Fig. 2. The flow from each flowmeter was channeled to an individual plenum and injected into the chamber through an injection slot or a perforated plate to be described in a subsequent paragraph.

Each of the injection configurations fabricated and tested was constructed to the same scale as that required for the spherical cavity. For all the configurations, the distance between plenums was 1.5 in. and the maximum distance from the axis of symmetry to the outer-wall was 6.0 in. For most of the outer-stream injection configurations, the chamber was constructed as a 60 deg wedge section. The apex of the wedge section is the equivalent axis of symmetry for the spherical cavity. The outer-stream injector was installed as part of a cylindrical section rather than as part of a spherical section. This approximation to a segment of a sphere significantly reduced the cost of fabricating an injection geometry compared to that required for the spherical cavity and, therefore, it was possible to test several outer-stream injection component geometries and to modify these geometries as required.

Sketches of two injection configurations are shown in Figs. 4 and 5. The geometry shown in Fig. 4 is a modified version of the Conical Wall Jet-III configuration which was tested in the spherical cavity (Ref. 14). The equivalent spherical cavity for this chamber had the following shape: (1) the upstream section (plenums 1 through 5) and downstream section (plenums 8 through 10) of this configuration were hemispherical in shape and (2) the

5

center section (plenums 6 and 7) had a cylindrical shape. The exhaust nozzle had a 90 deg included angle conical shape and was connected to the return line. The following modifications were made to the basic conical wall jet geometry: (1) the injection geometry for plenum 1 was changed several times; (2) the geometry for plenums 2 and 3 was modified by increasing the number of vanes from 2 to 7 and 9 per plenum, respectively; (3) a 60 deg conical vane ('coolie hat' shape) similar to that employed at Idaho Nuclear Corporation was installed upstream of the inner-stream injection; and (4) the slots were filled with corrugated metal ribbon or sections of honeycomb. The equivalent spherical shape of Configuration III, shown in Fig. 5, had annular and conical wall jet injectors. The conical wall jet injectors for plenums 2, 3, 8, 9, and 10 were similar to those employed in the previous wall jet geometries. However, the flow from plenums 4, 5, 6, and 7 was directed axially without any radial component. In addition, the slot area for plenums 4 through 10 was about one-half that previously employed with the ratio of the slot opening to the axial length equal to $1/(12)$. For some of the tests, the slots had a corrugated metal ribbon insert to promote small-scale three-dimensional mixing.

Wall jet injection vanes, similar to those proposed for use in the NASA-SNPO Fission Cavity experiment, were designed and fabricated at NASA Lewis Research Center for testing at UARL as part of the present program. These vanes were designed for plenums 2 through 5 of the hemispherical-cylindrical chamber (Fig. 4). The LRC vanes, installed in the test chamber, are shown in the photograph of Fig. 6. Each of the LRC vanes consist of rectangular slots of width of 0.070 in. and length 0.040 in. separated by a divider of 0.12 in. For an equivalent spherical-shaped cavity, the wall shape covered by the vanes is a hemispherical shape covering the upstream portion of the chamber. The shape of the downstream section of the chamber was that of Configurations I and II. Corrugated metal ribbon was inserted into the injection slots of plenums 5 through 10.

The flow structure for each combination of configuration and flow condition was recorded by photographing the chamber a short time period after dye was injected at one of the ten dye injection locations. For the photographs shown in this report, an exposure of 1/50 second was used. A plane through the center of the chamber was illuminated by means of a BH6 mercury lamp, a 10 in. diameter focusing lens, and a 1/4 in. slot along the length of the chamber. Thus, a cross section of the chamber could be viewed and evaluated.

From the coaxial-flow tests of Refs. 4, 8, and 10, it was determined that decreasing the turbulence scale and intensity of the flow in the shear layer between the outer-stream and inner-stream gases at the test chamber injection location would result in significant increases in the amount of inner gas contained in the cavity compared to conventional techniques of injecting coaxial streams into a chamber. Previous film cooling studies have also shown that the mixing near the wall is a function of the injector geometry (e.g., Ref. 17). These studies were directed toward preventing mixing between streams and maintaining the flow direction and velocity of the injected fluid. However, in the spherical cavity with a small diameter inner-stream source, the fluid mechanics requirement is that the inner-stream fluid must flow from the source and fill a large fraction of the cavity without significantly mixing with the outer-stream fluid. Whether the inner-stream fluid flows from the injector to fill the central region of the cavity or mixes with the outer-stream fluid and/or is convected to the cavity exhaust is dependent on the gravitational effects, the entrainment or mixing rate between the outer-stream and inner-stream fluids, the cavity shape, and the injection flow rate and velocity distributions for both streams. For the previous spherical cavity tests (Ref. 14) with air as the inner gas, the inner stream was entrained by the outer stream too rapidly with the result that the center of the chamber was filled with low-concentration inner gas. For the previous tests (Ref. 14) with Freon-11 as the inner gas, the Freon-11 was accelerated by the buoyancy effects toward the exhaust nozzle with the result that the inner-gas concentration was high only along the axis of symmetry. The dilemma to be solved is that a heavy inner gas such as Freon-11 must be forced to fill the chamber without dilution. This problem currently has the additional constraint that no structure can exist with the cavity except for the spherical inner-stream porous injector which simulates the vaporized nuclear fuel. Following is the discussion of the contract effort in this endeavor.

The flow structure was photographed for a total of forty-one flow conditions during the outer-stream component development test program. These were conducted for twelve different wedge configurations and one flat configuration. During the initial test period with the flat and wedge configurations, the flow with the chamber was found to be different between the two configurations for identical flow rates from the plenums. One difference was the tendency of the flow to recirculate in the wedge-shaped cavity and flow toward the exhaust duct in the flat cavity. As a result, only the wedge-shaped configuration was used for subsequent tests. This was done because the wedge is a good approximation to a fraction of the sphere and because the results from the first wedge-shaped configuration generally agreed with those obtained in gas tests in a similarly shaped spherical cavity. The

construction details of the wedge-shaped outer-stream injection configurations
are given in TABLE I and shown in Figs. 4, 5, and 6. The flow conditions for
each of the tests in the wedge-shaped test sections are shown in TABLE II.
The test configuration, the flow ratio, W_o/W_i, the Chamber Reynolds number,
Re_c, and the percent of the total outer-stream flow from each plenum is given
for each Run Number.

A series of tests was conducted with Chamber IIA to determine the effect
of changes in Reynolds number on the flow field. Tests (W10, W11, and W12)
were conducted with approximately uniform flow from plenums 2 through 10 at
25, 50, and 100 percent meter capacity. The equivalent spherical cavity
Reynolds number for these flow rates was 22,000, 48,000, and 93,000. There
was no discernable effect of the injection flow rate on the flow pattern.
The conclusion from this result was that for this flow range, the effect of
Reynolds number was negligible and, consequently, the remaining tests were
conducted at a Reynolds number of approximately 50,000, the Reynolds number
specified for the one- and two-component gas tests to be conducted in the
spherical cavity.

The tests with Configurations IB and IIB were conducted to determine the
effect of inserting honeycomb into the slots. The flow near the injection
wall in the downstream region of these two chambers appeared the same.
However, the turbulent mixing appeared to be less intense for Configuration
IIB. As a result, the number of injection slots per plenum for plenums 1, 2,
and 3 were increased and the width of these injection slots was decreased for
the subsequent tests in Chamber I. As a result of this change to add more
injection slots in the upstream plenums, the shear layer between the outer-
stream and inner-stream fluid became more two-dimensional with a well-defined
vortex wave structure typical of laminar or low-turbulence-intensity shear
layers (e.g., Refs. 6, 8, and 9). Most of the differences which occurred in
these preliminary tests were difficult to record photographically and,
consequently, photographs are not shown.

Because the flow characteristics for tests W10, W11, and W12 were
unaffected by changes in the cavity Reynolds number, the total outer-stream
injection flow rate was held approximately constant for the subsequent tests.
However, the flow rate through each plenum, and the inner-stream flow rate
were varied. The effect of these changes for Configurations IF, IIIB, and
IVA are shown in Figs. 7, 8, and 9. For these configurations, the flow from
plenum 1 (upstream end) was injected through a perforated screen. The flow
characteristics observed in nine tests (W29, W28, W31, W35, W36, W39, W34,
W32, and W37) included a large eddy structure with almost circular shapes
(1 to 2 in. dia) in the central region of the test chamber and an elongated
roll-shape near the outer-stream injectors. For the same injection flow

distribution, the flow in Configuration IVA had more of a tendency to recirculate in the central region than the flow for chambers IF and IIIB. This was attributed to the higher injection velocities from plenums 2 through 5 for Configuration IVA which occurs because of the small wall jet size and the smaller number of wall jets for Configuration IVA (see TABLE I). No difference in the size of the turbulent boundary layer can be discerned between these configurations and all appear to have the same shear layer vortex rolls between the wall jet boundary layer region and the cavity region (shown best in photograph with dye injector from plenum 2).

Tests were conducted in Chambers I and III with the flow from plenum 1 , injected from the wall jets rather than from the perforated plate (discussed in the previous paragraph). Results from these tests with Configurations IE and IIIC are shown in Figs. 10 and 11. The significant difference between these tests and those conducted with injection from plenum 1 through a perforated plate is that the inner-stream flow is entrained closer to the peripheral wall in the plenum 1 and plenum 2 region. This flow characteristic is required for the gas tests with Freon-11 as the inner gas. For a flow ratio, W_o/W_i, equal 21, and the outer-stream flow rate increasing from the upstream to the exhaust end of the cavity, the inner-stream fluid for Configuration IE flows into a recirculation cell while the inner-stream fluid for Configuration IIIC flows toward the peripheral wall at all the axial locations (i.e., no recirculation cell). This result was a major factor in selecting Configuration IIIC to be fabricated inthe spherical cavity for use in the gas tests.

The distance from plenum 1 where the inner-stream injector was located was also varied. The center of the inner-stream injector was opposite plate 3-4 for Configuration IE and plate 2-3 for Configuration ID. For the same inner-stream and outer-stream flow rates, the flow patterns within Configuration ID (Fig. 12, Run No. 21) includes a recirculation cell, whereas the inner-stream flow within Configuration IE (Fig. 12, Run No. 25) is toward the peripheral wall at all axial locations. The conclusion from this comparison is that the inner-stream injector location significantly influenced the cavity flow patterns. Consequently, the spherical cavity inner-stream injector plumbing was modified such that the injector location could be adjusted without disassembling the cavity.

A 60 deg vane was also installed adjacent to the inner-stream injection location to determine the effect on the mixing near the inner-stream injection location. A comparison of the flow structure for Runs 16 and 21 (Fig. 12) shows that the structure of the shear layer vortices with the vane are similar to those that occur without the vane. The conclusion from these tests was that the wave structure was not significantly influenced by the vane.

The principal conclusion from these flow visualization tests was (1) that the cavity shape, the wall-jet area distribution, the outer-stream injection distribution, and the flow ratio, W_o/W_i, all significantly affect the inner-stream flow pattern and would, therefore, affect the inner-gas containment in the spherical cavity tests. In addition, (2) use of corrugated metal ribbon inserts in the downstream plenums did not appear to affect the wall jet characteristics. However, preliminary tests showed that (3) use of several wall jets with a corrugated metal insert for plenums 1 through 4 provided a wall jet region with smaller scale turbulence than for wall jets without inserts. Finally, (4) injecting from plenum 1 through wall jets at 20 deg to the local surface tangent caused the inner-stream flow to be entrained closer to the upstream cavity wall than injecting through a perforated plate. These characteristics will be useful for the spherical cavity tests with Freon-11.

FLOW FIELD CALCULATIONS

Streamlines and concentration contours were calculated for a flow within a cavity similar to that employed for the one- and two-component gas tests. The injection distribution for the outer-stream gas and the inner-stream gas were approximately those employed in previous and concurrent gas tests. The flow field within the cavity was calculated for various combinations of four outer-stream injection distributions, inner-stream to outer-stream gas density ratios of 4.7 and 1.0, Schmidt numbers of 1.0 and 10, kinematic viscosities of 1.0, 0.1, and 0.03 ft^2/sec, and gravitational fields of -1, 0, 1, and 100 times the earth's gravitational field. Results are presented to show the effect of changes in each variable on the flow field calculated for the arbitrarily selected Standard Condition.

Description of Numerical Method

The procedure used for these calculations is a modification of the Basic Computer Program described in Ref. 18. For this procedure, the Navier-Stokes equations are formulated in finite-difference form as first order equations with the stream function, the vorticity, and the mass concentration of the inner-stream gas as the dependent variables. These equations are solved subject to the boundary conditions by an iterative method of successive substitutions.

The cylindrical coordinate grid field used for the calculations is shown on the right side of Fig. 13. The boundary grid points marked "0" are close to the equivalent wall jet locations shown on the left side of Fig. 13. The calculation boundary conditions approximate a hemisphere shape for plenums 1 through 5, a circular cylinder shape for plenums 6 and 7, a portion of a hemisphere for plenums 8, 9, and 10, and a 90-degree-included-angle conical exhaust section for the region downstream of plenum 10. The streamline distribution at the "X" and "0" locations was calculated from the outer-stream injection velocity and injection angle specified in TABLE III. Because a cylindrical coordinate system was employed for these calculations, the boundary grid points for the upstream and downstream hemispherical sections do not lie on the hemispherical radius. The boundary condition stream functions were calculated for the grid points "0" and "X" in the hemispherical section by (1) using the stream function relationships for spherical flow, (2) the specified relationships for the local radial and tangential velocities on the hemispherical surfaces, and (3) by assuming inviscid flow occurred between the hemispherical shell and each of the adjacent grid points. The boundary condition in the exhaust nozzle was that for a no-slip boundary. The stream function for the inner-stream injector was calculated for a uniform radial flow from a 2 in. diameter porous sphere, which is almost identical to the gas test boundary condition where a 2 in. diameter porous sphere is fed by a 7/8 in. diameter tube. The inner-stream and outer-stream flow rates were constant for all calculations at 0.01 and 0.50 lb/sec, respectively. The temperature and chamber pressure of the gases were fixed at 180 deg F and 13.9 psia, respectively, for all calculations. The radial component of the velocity and radial gradient of the concentration profiles were specified to be zero along the axis of symmetry and the axial gradients of all the components were specified to be zero at the exhaust location, six grid points downstream of the exhaust duct grid location shown in Fig. 13.

Discussion of Results

The streamline and inner-gas concentration distributions within the chamber were calculated for the four injection distributions given in TABLE III. The flow conditions were selected because they are similar to those which were tested in the spherical cavity tests of Ref. 14. The total outer-stream flow rate and the inner-stream flow rate for all these calculations were maintained constant while the outer-stream injection flow angle and the flow rate per outer-stream injection surface area were varied.

The flow condition chosen as the Standard Condition had the Case IV outer-stream injection distribution; that is (1) the velocity component perpendicular to the hemispherical and cylindrical peripherall wall surfaces was

constant with the result that the injection flow rate per unit length (dW_O/dZ) was constant, (2) the injection flow angle (α) relative to the surface was varied from radial (90 deg) at the most upstream location to an angle with a tangent equal 1/6 at the end of the upstream hemispherical section, and (3) the flow angle was maintained at α = arc tan (1/6) for the cylindrical and downstream hemispherical sections. The α = arc tan (1/6) corresponds to two 1/8 in.-wide injection slots per plenum, $1\frac{1}{2}$ in. apart, a geometry which was employed during previous gas tests, Ref. 14. For the other injection conditions, Cases V, VI, and VII, the injection angle distribution was the same as for Case IV or was held constant at α = arc tan (1/6) and the outer-stream flow rate per unit axial length was either held constant as in Case IV or was varied linearly from a value 1/2 the average rate at the upstream end of the cavity to a value of $1\frac{1}{2}$ the average at the downstream injection location. The fluid properties and gravitational field for the Standard Condition were as follows: the ratio of inner-stream gas density to outer-stream gas density was equal 4.7, the kinematic viscosity was equal 0.1 ft^2/sec (approximately 500 times the molecular viscosity of air), the Schmidt number was equal 1.0, and the gravitational field had the acceleration toward the exhaust nozzle with a value of 32 ft/sec^2 (i.e., the earth's field). For a gas density ratio of 4.7, this flow condition resulted in a greater amount of inner gas being contained within the cavity than any other flow condition calculated for this study.

The calculated streamline and inner-gas partial pressure contours for the Standard Condition are shown in Figs. 14 and 15, respectively. The streamlines correspond to the percent of the total injected flow. The 2 percent streamline (No. 7) emanates from the upstream edge of the inner-gas injector. For this flow condition, the zero streamline (No. 9) lies along the axis of symmetry from the downstream edge of the inner-stream injector through the exhaust nozzle. A small recirculation cell occurs for the one percent streamline (No. 8). This flow structure is attributed to the interaction of the flow near the peripheral wall and the flow from the inner-stream injector. A unique feature of this flow condition is that the 2 percent streamline (No. 7) encompasses the recirculation cell. The concentration profiles, i.e., the inner-gas partial pressure profiles, for the Standard Condition show that concentrations greater than 30 percent occur only within a spherical source radius of the axis of symmetry. The streamlines emanating from the source flow axially toward the exhaust nozzle and decrease in concentration of inner-stream gas. The decrease in the inner-stream gas concentration in the recirculation cell region was more rapidly diluted by diffusion to the adjacent streamlines than for the flow along the axis. The result was that the average inner-gas partial pressure within the chamber is only 4 percent of the total pressure, considerably less than required for the operation of the full-scale gas-core nuclear rocket engine.

The effect of the outer-stream injection distribution on the streamline and concentration distribution is shown in Figs. 16 and 17. For the Case V, VI, and VII injection conditions, a recirculation cell, considerably stronger than that of Case IV, occurs in the upstream portion of the cavity. The strongest cells, Cases V and VII, have a recirculation flow rate greater than 10 percent of the total flow through the cavity (Line No. 13). For Cases V, VI, and VII, all the flow from the inner-stream injector is swept upstream and toward the peripheral wall where the velocity and concentration gradients are high. The result is that the average inner-gas partial pressure for these flow conditions is 1/3 to 1/2 that of Case IV where the flow from the inner-gas source flows downstream and radially outward.

For the Case IV outer-stream flow distribution, the flow was calculated for a kinematic viscosity of 0.03, 1.0, and 0.1 ft^2/sec. The results of these three calculations are shown in Figs. 18 and 19. For a viscosity of 1.0 ft^2/sec, the flow has a recirculation cell with more than twice the flow rate of the inner-stream injector. The cell for the 0.1 ft^2/sec case (Standard Condition) is recirculating flow at less than the inner-stream flow rate. For the 0.03 ft^2/sec case, the recirculation cell has approximately the same flow rate as the 0.1 ft^2/sec case; however, the cell is outside the streamlines emanating from the inner-gas source. The concentration distribution profiles in Fig. 19 show the effects of these flow patterns. The 1.0 ft^2/sec case has the inner gas concentrated near the gas injector and the 0.03 ft^2/sec case has the high concentration regions concentrated very close to the axis of symmetry. The result is that the average partial pressure of inner gas within the chamber is greater for the 0.1 ft^2/sec case than either the 0.03 or the 1.0 ft^2/sec cases. The conclusion is that for the 0.1 ft^2/sec case, the tendency of the flow to recirculate is balanced by the gravitational forces which tend to accelerate the heavier gas toward the exhaust nozzle. Although the maximum inner-gas containment will probably occur for a value ν other than those selected, the tradeoff between viscous and gravitational forces has been shown. The turbulent spherical cavity Reynolds numbers, $Re_{s,t} = 4 W_o/(\pi D \rho_o \nu_t)$ were 10, 100, and 333 for the $\nu = 1.0$, 0.1, and 0.03 ft^2/sec cases, respectively.

Calculations were also performed to determine the effects of gravity or buoyancy on the streamline and concentration contours within the spherical cavity for the Case IV outer-stream flow distribution. These calculations were for gravity fields of one upward, zero, one downward (Standard Condition), and 100 downward times the earth's gravitational field. The results are shown in Figs. 20 and 21. The most pronounced change from the Standard Condition (g = one downward) is for the g = 100 downward case with the Buoyancy number, B = 150. For the B = 150 case, the streamlines emanating from the inner-gas source drop toward the exhaust nozzle without diverging.

13

For all four flow conditions, an annular recirculation cell occurs in the central portion of the cavity. The shape of the recirculation cell is a function of gravitational field and direction. The density contours for the 0, +1, and -1 gravitational fields are approximately the same. However, there is a slight decrease in the average-partial pressure of inner gas from 0.045 for the -1 'g' field to 0.040 for the +1 'g' field (Standard Condition). For the +100 'g' field, the high concentration contours are close to the axis of symmetry and the average inner-gas partial pressure ratio is 0.011.

The flow field was also calculated for a flow with the inner gas at the same density as the outer gas. This change influences three parameters: (1) the dynamic viscosity which is the product of the local density and the kinematic viscosity, ν (ν held constant), (2) the volume flow rate from the inner-gas source because the weight flow rate was held constant, and (3) any gravitational effects. The streamline and concentration contours obtained from these calculations are shown in Fig. 22. The principal change from the Standard Condition is that the streamlines emanating from the inner-gas source lie inside the annular recirculation cell. It was anticipated that because of the larger volume flow for the constant density gas, the streamlines from the inner-gas source would encompass the recirculation cell. Because the gravitational effects were shown to be small for the Standard Condition, this anomalous result is attributed to the change in viscosity in the central portion of the cavity. For the constant density case, the average partial pressure ratio is increased by a third to 0.053 from the Standard Condition value of 0.040.

The effects of increasing the Schmidt number from one for the Standard Condition to ten on the streamline and concentration contours are shown in Fig. 23. The streamline profiles are almost identical for the two cases. However, the concentration profiles for the Schmidt number equal ten case are closer to the axis of symmetry than for the Schmidt number equal one (Standard Condition) case. The result is that the average partial pressure ratio is decreased from the value of 0.040 for the standard condition to 0.037. Thus, the effect of gravity counteracts the decreased diffusion by accelerating the inner-gas flow toward the exhaust nozzle.

The solutions of the Navier-Stokes equations for the spherical cavity flow problems described in the previous paragraphs show the complex relationship between changes in the boundary conditions or fluid properties and the streamline and inner-gas concentration contours which occur within the cavity. (1) Changes in the outer-stream injection flow rate per unit area, the injection angle, and the fluid viscosity had large changes in the cavity flow patterns. In addition, (2) increasing the gravitational field, or the buoyancy parameter, showed that adverse changes in the inner-gas containment could

be obtained for the selected flow condition. The calculated streamline and concentration contours had the general characteristics observed experimentally in previous and concurrent one- and two-dimensional gas tests. However, in order to quantitatively rather than qualitatively predict flow patterns and concentration distributions, existing turbulent transport models will have to be improved and verified for a range of cavity configurations, injection configurations, and flow conditions. The present calculation procedure using a cylindrical coordinate system appears to be satisfactory for the present 'spherical' cavity flow problem with a small diameter inner-gas source and an exhaust nozzle.

ONE- AND TWO-COMPONENT GAS TESTS

Qualitative one- and two-component gas tests were conducted previously (Ref. 14) with outer-stream injection geometries similar to those employed in the Outer-Stream Injection Component Development Tests. These tests were discussed in the Background Information section. One of the objectives of the present study was to obtain quantitative measurements of the inner gas contained within the spherical cavity. During the mass spectrometer check-out phase of the present effort, a concentration measurement was obtained which indicated that the amount of inner gas contained within the chamber had been overestimated in Ref. 14. As a result, the Outer-Stream Injection Component Development Tests and the Flow Field Calculations were carried out before additional concentration measurements were obtained in one- and two-component gas tests. Following is a summary of the results of the flow visualization tests and the concentration measurement tests which were conducted subsequent to the Outer-Stream Injection Component Tests and the Flow Field Calculations.

Description of Equipment and Procedures

Equipment. - A photograph of the spherical cavity test apparatus employed in the major portion of this study is shown in Fig. 24. Two gas streams were supplied to this apparatus: an inner stream to simulate the gaseous nuclear fuel and an outer stream to simulate the propellant. The inner stream was ducted directly to the inner-gas injector which was attached to the vertical tube shown in Fig. 25 at the upper end of the disassembled cavity. The outer stream was ducted through variable area flowmeters, valves, and hoses to the plenum chamber inlet ducts. The outer-stream injection configuration was attached to plates separating the plenums in Fig. 25. To supply the desired combinations of inner-jet and outer-stream gases and gas

weight-flow rates to the test apparatus, a combination of gas generators, heaters, and compressors were used. Airflow for the outer stream was drawn into the cavity using the Laboratory vacuum system. The total flow rate for the outer stream was measured with a nozzle located in the outer-stream supply lines. The inner-stream gas flow rate was measured with a variable are flow-meter. The outer stream was heated to approximately 203 deg F (95 deg C) using the 'light gas' supply system described in Ref. 19. The inner-jet gases used were air and Freon-11. The air was obtained from the 400 psi (2.76×10^6 Nt/m^2) air supply and heated to 250 deg F (120 deg C) in a conventional tube-and-shell heat exchanger. The Freon-11 was vaporized on the shell side of a tube-and-shell heat exchanger and superheated in the air superheater. The average cavity pressure was approximately 14 psia (9.3×10^4 Nt/m^2).

   Injection Configuration. - A sketch of Spherical Cavity VB used for the inner gas concentration measurement tests is shown in Fig. 26. The wall jets for plenums 2 through 10 have 1/8-in.-thick slots with a 0.003-in.-thick, 0.038-in.-wide corrugated metal ribbon insert. The corrugated metal ribbon was used to promote small-scale three-dimensional mixing. Lexan sheet (a clear transparent plastic with a softening temperature higher than Lucite) 0.03 in.-thick was used for the cavity wall lining to obtain flow visualization of the cavity flows. Flow from plenums 4 through 10 was injected through a single slot. The number of slots per plenum was increased to 2, 3, and 6 for plenums 3, 2, and 1, respectively, to obtain larger injection areas. The walls of plenum 1 were 0.020-in.-thick stainless steel sheet. The Spherical Cavity VB was used for the flow visualization tests and the inner-gas concentration measurement tests documented in this section. Additional exploratory tests were conducted with Spherical Cavity VA which was identical to Cavity VB except that the flow from plenum 1 was injected through a 25 percent open perforated plate with 0.020 in. dia holes rather than the six radial wall jets shown in Fig. 26. The inner-stream injector consisted of a 2 in. dia porous ceramic sphere mounted on a 7/8 in. outside diameter stainless steel tube. The sphere was constructed of two hemispheres with 1/4-in.-thick walls by the Coors Corporation from their P-100 porous ceramic material. The axial location of the inner-stream injector could be positioned from outside the chamber in order to determine an optimum injection location.

   Flow Visualization Procedures. - A schematic of the optical system used for the flow visualization photography of the containment tests is shown in Fig. 27. Light was supplied by tungsten-halogen (bromine) quartz lamps and diffused with drawing vellum to provide uniform background illumination. Iodine was used to color the inner-jet gas for all of the flow visualization tests. For the black and white photographs, light to the films was filtered at a wavelength absorbed by the iodine vapor to obtain good contrast between

the regions with and without iodine colored inner gas. Type 7241 EF Kodak
Ektachrome film was used for all motion pictures obtained. Film sequences
were obtained with Fastax and Miliken cameras at 24 to 500 frames per second.

Concentration Measurement Procedures. - The inner-gas concentration
measurements were obtained with a UARL-owned Time-of-Flight Mass Spectrometer
manufactured by the Bendix Corporation using the apparatus shown in Fig. 28.
When air was used as the inner gas, the inner-gas concentration was obtained
by using argon as a trace gas. A 10 percent mole fraction of argon in the
inner gas mixture allowed the inner-gas concentration to be determined within
0.01 mole fraction or 10 percent of the local value, whichever was greater.
The mass spectrometer was calibrated with known air-argon samples before and
after the inner-gas concentration measurement tests. The concentration of the
argon upstream of the inner-jet stream injector was monitored before and after
the radial traverse at each axial location. Gas samples were obtained at
eleven or more radii for nine axial locations at the axial midplane of each
plenum from plenum 2 to plenum 10 (see Fig. 26). For the tests with Freon-11
as the inner gas, the mass spectrometer was also calibrated before and after
the tests without changing any portion of the test apparatus. This calibra-
tion effort was required because the Freon-11 and air molecules have greatly
differing molecular weights which causes them to have different loss coeffi-
cients when flowing through the mass spectrometer system.

Discussion of Flow Visualization Tests

Flow visualization tests were conducted after the assembly of Spherical
Cavity Configurations VA and VB to determine the outer-stream flow distribu-
tion for which the greatest amount of inner gas appeared to be in the cavity
for each flow ratio, W_o/W_i. These tests were qualitative and subjective
because (1) the concentration of iodine vapor carried by the inner gas varied
for each flow ratio, and (2) the variation of the total amount of inner gas
within the chamber with changes in the outer-stream flow distribution was
difficult to discern. The flow visualization tests were initiated with a
series of tests conducted in Spherical Cavity VA. The flow patterns obtained
with air as the inner gas were like those obtained in the Outer-Stream
Injection Component Development Tests with water as both the inner- and
outer-stream fluid. The conclusion from these tests with air as the inner-
stream gas was that the flow patterns obtained in the wedge-shaped test cham-
ber with water as the working fluid were approximately the same as those
obtained in the spherical cavity at the same flow ratios, W_o/W_i. However,
with Freon-11 as the inner gas, the outer-stream flow rate could not be

adjusted to obtain a cavity full of inner gas at the flow ratios specified for these tests, namely W_o/W_i = 25, 50, or 100. Consequently, Cavity V was modified to include six radial wall jets of Cavity VB.

A series of exploratory tests was also conducted with Spherical Cavity VB. Although the greatest apparent inner-gas containment that could be obtained with air as the inner gas was less than or equal to that obtained for Spherical Cavity VA at the same flow rates, the apparent inner-gas containment with Freon-11 as the inner gas was greater. Consequently, Cavity VB was selected for the inner-gas concentration measurement tests. The outer-stream flow distribution for all the tests with Freon-11 as the inner gas was adjusted until a portion of the Freon-11 was in a recirculation cell and a portion was accelerated along the axis of symmetry toward the exhaust nozzle. This flow pattern was selected because the greatest calculated inner-gas containment was obtained when this flow pattern was obtained. The experimentally obtained flows were unstable in that the location of the recirculation cell would progress about the axis of symmetry in a spastic manner. For tests with air as the inner gas, the outer-stream flow distribution for which the greatest apparent inner-gas containment was approximately the same for the three flow ratios, W_o/W_i = 25, 50, and 100, and is shown in Fig. 29. For tests with Freon-11 as the inner gas, the best apparent inner-gas containment for each flow rate was obtained by increasing the outer-stream flow rate for plenums 1 and 2 as the inner-stream flow rate, W_i, was increased. The outer-stream flow rate for the tests with Freon-11 are also presented in Fig. 29.

One second time-exposed photographs of the iodine vapor within the chamber with air and Freon-11 as the inner-stream gas are shown in Fig. 30. The flow visualization results for air as the inner gas show higher concentrations in the cavity for tests with W_o/W_i = 25 compared to W_o/W_i = 50 and 100. The flow pattern with W_o/W_i = 50 and 100 included a recirculation cell, although the regions filled by the inner gas for all three cases appear to be about the same. However, for tests with Freon-11 as the inner gas, the region filled with inner gas appears larger for W_o/W_i = 25 than for W_o/W_i = 50 and 100. From the high-speed motion pictures, it was apparent that the high concentration of the Freon-11 inner gas was shifting location in an unstable manner for W_o/W_i = 50 and 100.

Discussion of Inner Gas Concentration Measurement Tests

The inner-gas concentration distribution within the Spherical Cavity VB was determined for the flow conditions shown in Fig. 30 using the Time-of-Flight Mass Spectrometer described in a previous subsection. Data were obtained at eight to thirteen locations along a single radius at the axial

midplanes of plenums 2 thorough 10. For Run 202, with air as the inner gas and W_o/W_i = 50, data were obtained along two radii 180 deg apart because the inner gas distribution was asymmetric for this flow condition. For Run 202, an average of the two profiles was used to determine the local and total inner-gas concentrations.

The concentration profiles for the tests with air as the inner gas are presented in Figs. 31 through 33. For W_o/W_i = 25, Fig. 31, the inner-gas concentration in the central portion of the cavity is high, $P_i/P > 0.8$. However, the concentration drops sharply at radii of 4.5 to 5 in. The conclusion from these results for W_o/W_i = 25 is that recirculation did not occur upstream of plenum no. 9 and that only a small amount of mixing between the inner-stream and the outer-stream gases occurred near the inner-stream gas injection location. For Run 202 with W_o/W_i = 50, high inner-gas concentrations were obtained near the axis of symmetry for plenums 3 (Injection Location) and 4. However, the concentration profiles for plenums 6 through 9 indicate that a strong recirculation cell occurred in those regions. The peak concentrations in the radial profile for the axial locations with the recirculation cell is less than 50 percent. The maximum concentration gradient in the recirculation zone is also less than that obtained for the W_o/W_i = 25 case with no recirculation upstream of the exhaust nozzle region. For Run 203 with W_o/W_i = 100, the local concentrations are lower than those obtained for the tests with W_o/W_i = 25 and 50. This is in agreement with the flow visualization results (Fig. 30).

The inner-gas concentrations obtained for tests with Freon-11 as the inner gas are presented in Figs. 34 through 36. For the tests with W_o/W_i = 25 and 50, the highest inner-gas concentrations were obtained along the axis of symmetry. However, for the tests with W_o/W_i = 100, a region of high inner-gas concentration occurs along the axial midplane radius of plenum 3 (the center of the inner stream injector).

The total average inner-gas partial pressure within the cavity was determined for each run by graphically evaluating the integral $\int_{-2}^{14} \int_0^6 (P_i/P) r dr\, dz$ and dividing by $1/(2\pi)$ times the volume within the cavity. The axial variation of the integral and the average inner-gas partial pressure ratio, $\int_0^6 (P_i/P) r dr$ results are presented in Fig. 37. The results from the tests with air as the inner gas show the expected decrease in concentration integral with increasing flow ratio, W_o/W_i. However, the results from the tests with Freon-11 as the inner gas show that average inner gas within the chamber was approximately the same for the three flow ratios. Approximately half the inner gas for W_o/W_i = 100 is contained in the plenum 3 region. If the high concentration region is narrower than a full plenum width, the integrals evaluated as straight lines from data point to data point will yield

19

a higher concentration for that run than actually existed. The anomolous results for the tests with Freon-11 as the inner gas indicate that the outer-stream flow rate distribution was probably not adjusted for the optimum containment.

COMPARISON OF ANALYTICAL AND EXPERIMENTAL RESULTS

A significant result from the computation of the flow fields within the spherical cavity was that a local maximum in the total inner-gas containment occurred when a portion of the inner gas was entrained into a recirculation cell and a second portion flowed directly toward the exhaust nozzle. This result was obtained for Freon-11 as the inner gas and was attributed to the balance between the gravitational forces accelerating the heavy inner gas toward the exhaust and the viscous shear forces which entrain flow from the central portion of the cavity and tend to recirculate the inner gas upstream. As a consequence of this result, the outer-stream flow rate distribution for each of the gas tests with Freon-11 as the inner gas was adjusted such that a portion of the inner gas entered a recirculation cell and a portion flowed toward the exhaust nozzle. Although the turbulent transport coefficients are unknown for the experimental tests and the outer-stream injection conditions are not identical for the analysis and the experiment, a comparison of the inner-gas concentration distribution results is useful because the flows for the central portion of the cavity were at least qualitatively similar.

A comparison of the calculated and measured inner-gas concentration pro-files is shown in Fig. 38 for a flow condition with W_o/W_i = 50 and Freon-11 as the inner gas. Other flow conditions for the analysis and the experiment are presented in the figure. The analytical results are for the Standard Condition discussed in the FLOW FIELD CALCULATIONS section and the experimental results are for Run 206 described in the previous section. The analytical and experi-mental concentration profiles at the axial centerline of plenums 2, 3, and 4 are similar in shape and magnitude. The trend toward decreasing maximum concentration with distance from the inner-gas injector is the same for both analysis and experiment; however, the peak value at each axial station and the shape of the profiles differ in that the experimental results are generally greater than the analytical results. The average inner-gas partial pressure ratio, i.e., the fraction of the cavity volume filled with inner gas, was 0.04 for the computed case and 0.06 for the experimental case. The conclusion from this comparison of the calculated and measured inner-gas distribution within the cavity is that the present calculation procedures predict the trends and flow characteristics encountered in the experimental

studies. However, additional effort will be required to obtain a general formulation for the turbulent transport quantities, i.e., turbulent viscosity and diffusion coefficients, before a flow condition can be calculated by specifying the scale and intensity of the turbulence at the injection location.

COMPARISON OF EXPERIMENTAL RESULTS WITH CURRENT REQUIREMENTS

The estimated inner-gas containment results obtained with the inner-gas injector adjacent to the upstream end of the chamber are compared in Fig. 39 with previous results from coaxial-flow studies and with the GNR open-cycle fluid mechanics requirements. The upper range of the present spherical cavity results with air as the inner gas are within the containment region of interest designated on the graph. However, the present spherical cavity results with Freon-11 as the inner gas are lower than recently deemed sufficient for use in the full-scale engine. These results are due in part to the buoyancy effects and may be significantly improved by designing a cavity which exhausts up rather than down. Further effort will be required to develop an injection configuration which is effective in producing desirable flow characteristics with the density ratio and buoyancy parameters expected in the full-scale engine.

SUMMARY OF RESULTS AND CONCLUSIONS

This experimental and analytical study of flow within a spherical cavity was directed toward obtaining higher average inner-gas concentration in the spherical cavity than obtained in previous studies. The outer-stream injection component development flow visualization tests and the calculation of the flow field within the spherical cavity were conducted prior to the inner-gas concentration measurement tests. Following are results and conclusions from the three phases of the program and a conclusion from a comparison of the present results with the engine requirements.

One- and Two-Component Gas Tests

1. For tests with air as the inner-stream gas, the maximum ratio of average inner-stream gas partial pressure to chamber pressure decreased from 0.40 for a flow ratio of outer-stream flow rate to inner-stream flow rate of 25 to an average inner-gas partial pressure ratio of 0.15 for a flow ratio of 100.

2. For tests with Freon-11 as the inner-stream gas, the maximum average inner-gas pressure ratio was constant at 0.07 for flow ratios of 25, 50, and 100 although the inner-gas distribution varied with flow ratio.

Flow Field Calculations

3. Changes in the outer-stream injection flow rate per unit area, the injection angle, and the fluid viscosity resulted in large changes in the streamline and concentration distribution within the cavity.

4. The calculated streamlines and concentration contours had the general characteristics observed experimentally in previous and concurrent one- and two-component gas tests.

5. The present calculation procedure using cylindrical coordinates provides an adequate system for calculating the flow within a spherical cavity with a small diameter inner-gas source. However, further work is needed to extend this to turbulent flow.

Outer-Stream Injection Component Development Tests

6. The cavity shape, the wall jet area distributions, the outer-stream injection distributions, and the ratio of the outer-stream flow rate to the inner-stream flow rate influenced the flow patterns within the cavity.

7. Injecting through wall jets at 20 deg to the local surface tangent caused a desirable flow where the inner-stream fluid flows close to the cavity wall in that region.

8. Use of corrugated metal ribbon inserts in the injection slots of the downstream section of the cavity did not affect the wall jet boundary layer characteristics in that region; however, use of these inserts in the upstream region decreased the scale and intensity of the turbulent eddies in that region which was desirable.

General Conclusion

9. Further development work is required to obtain desirable simulated-fuel containment characteristics in the spherical cavity with a small diameter source with ratios of simulated-fuel density to simulated-propellant density greater than one.

REFERENCES

1. Weinstein, H. and R. G. Ragsdale: A Coaxial Flow Reactor - A Gaseous Nuclear Rocket Concept. Preprint 1518-60, American Rocket Society, Inc., 1960.

2. Thom, K. and R. T. Schneider (eds.): Research on Uranium Plasmas and Their Technological Applications. Proceedings from Symposium held at Gainesville, Florida, January 7-8, 1970. NASA SP-236, 1971.

3. Ragsdale, R. G., et al.: Second Symposium on Uranium Plasmas: Research and Applications. Proceedings from Symposium held at Atlanta, Georgia, November 15-17, 1971. American Institute of Aeronautics and Astronautics, 1971.

4. Johnson, B. V.: Experimental Study of Multi-Component Coaxial Flow Jets in Short Chambers. NASA Contractor Report CR-1190, October 1968. First issued as United Aircraft Research Laboratories Report G-910091-16, April 1968.

5. Michalke, A.: On Spatially Growing Disturbances in an Inviscid Shear Layer. Journal of Fluid Mechanics, Vol. 23, Part 3, pp. 521-544, 1965.

6. Freymuth, P.: On Transition in a Separated Boundary Layer. Journal of Fluid Mechanics, Vol. 25, Part 4, pp. 683-704, 1966.

7. Clark, J. W., R. C. Stoeffler, and P. G. Vogt: Research on Instabilities in Atmospheric Flow Systems Associated with Clear Air Turbulence. United Aircraft Research Laboratories Report H910563-9, prepared under NASA Contract, June 1969.

8. Johnson, B. V.: Exploratory Experimental Study of the Effects of Inlet Conditions on the Flow and Containment Characteristics of Coaxial Flows. NASA Contractor Report CR-107051, September 1969. First issued as United Aircraft Research Laboratories Report H-910091-21, September 1969.

9. Johnson, B. V.: Analytical and Experimental Study of Spatially Growing Disturbances in Shear Layers Between Parallel Streams. Ph.D. Thesis, University of Connecticut, 1971. Also issued as United Aircraft Research Laboratories Report UAR-L124, July 1971.

REFERENCES (Continued)

10. Bennett, J. C. and B. V. Johnson: Experimental Study of One- and Two-Component Low Turbulence Confined Coaxial Flows. NASA Contractor Report CR-1851, 1971.

11. Ragsdale, R. G. and C. D. Lanzo: Summary of Recent Gas Core Reactor Fluid Mechanics Experiments. NASA Technical Memorandum NASA TM X-1847, 1969.

12. Kunze, J. F., D. H. Suckling, and C. G. Cooper: Flowing Gas, Non-nuclear Experiments on the Gas Core Reactor. NASA Contractor Report CR-120824, February 1972, prepared by Aerojet Nuclear Company under Contract C-59718B.

13. Ragsdale, R. G. and F. E. Rom: Gas-Core Reactor Work at NASA/Lewis. NASA Technical Memorandum NASA TM X-52309, 1967.

14. Johnson, B. V.: Exploratory Study of the Effects of Injection Configurations and Inlet Flow Conditions on the Characteristics of Flow in Spherical Chambers. NASA Contractor Report CR-1965, January 1972. First issued as United Aircraft Research Laboratories Report J910963-14, April 1971.

15. Ragsdale, R. G.: Relationship Between Engine Parameters and the Fuel Mass Contained in Open-Cycle Gas-Core Reactor. NASA Technical Memorandum NASA TM X-52733. Presented at Symposium on Research on Uranium Plasmas and Their Technical Applications, Gainesville, Florida, January 7-9, 1970.

16. Ragsdale, R. G.: Some Fuel Loss Rate and Weight Estimates of an Open-Cycle Gas Core Nuclear Rocket Engine. NASA Technical Memorandum NASA TM X-52775. Presented at AIAA Joint Specialist Conference, San Diego, California, June 15-19, 1970.

17. Sivasegaram, S. and J. H. Whitelaw: Film Cooling Slots: The Importance of Lip Thickness and Injection Angle. Journal of Mechanical Engineering Science, Vol. 11, No. 1, 1969.

18. Gosman, A. A., William Pun, A. K. Runchal, D. B. Spalding, and M. Wolfstein: Heat and Mass Transfer in Recirculating Flows. Academic Press, New York, 1969.

19. Kendall, J. S., A. E. Mensing, and B. V. Johnson: Containment
    Measurements in Vortex Tubes with Radial Outflow and Large Superimposed
    Axial Flow. NASA Contractor Report CR-993, March 1968. First issued
    as United Aircraft Research Laboratories Report F-910091-12.

LIST OF SYMBOLS

B Buoyancy parameter, $\left[(\rho_i - \rho_o)Dg/(\rho_i^2 U_i^2)\right]^{\frac{1}{2}}$

D Maximum diameter of cavity, ft (m)

g Gravitational constant, 32 ft/sec^2 (9.80 m/sec^2)

L Axial injection length within cavity, ft (m)

P Cavity pressure, lb/ft^2 (Nt/m^2)

P_i Local inner-gas partial pressure, lb/ft^2 (Nt/m^2)

$\overline{P_i}$ Average inner-gas partial pressure, lb/ft^2 (Nt/m^2)

r Local radius, ft (m)

R Maximum radius in chamber or spherical cavity, ft (m)

Re_c Water flow visualization chamber Reynolds number, $12\,W_o/(\pi R \mu_o)$

$Re_{S,L}$ Spherical cavity Reynolds number based on molecular viscosity, $4\,W_o/(\pi D \mu_o)$

$Re_{S,T}$ Spherical cavity Reynolds number based on turbulent eddy viscosity, $4\,W_o/(\pi D \rho_o \nu_T)$

U_r Radial injection velocity at cavity wall, ft/sec (m/sec)

U_θ Tangential injection velocity at cavity wall, ft/sec (m/sec)

W_F Weight-flow rate of simulated fuel, lb/sec (kg/sec)

W_I Weight-flow rate of inner-jet gas, lb/sec (kg/sec)

W_O Weight-flow rate of outer-stream gas, lb/sec (kg/sec)

W_P Weight-flow rate of simulated propellant, lb/sec (kg/sec)

Z Dimensionless cavity axial location, Z/L

Z^* Axial distance from upstream wall, ft (m)

α Angle between wall jet injection and local tangent to wall surface, deg

Θ Azimuthal location, deg

μ_o Dynamic viscosity of outer stream fluid, lb/sec-ft (kg/sec-m)

ν Kinematic viscosity, ft^2/sec (m^2/sec)

ρ Local gas density, lb/ft^3 (kg/m^3)

ρ_i Inner-gas density, lb/ft^3 (kg/m^3)

ρ_o Outer-stream gas density, lb/ft^3 (kg/m^3)

ϕ Mass fraction concentration of inner gas, ρ_i/ρ

ψ Stream function, lb/sec (kg/sec)

ω Vorticity function, 1/sec

TABLE I

CONSTRUCTION DETAILS OF OUTER-STREAM INJECTION COMPONENT CONFIGURATIONS

Config-uration	Type Injector for Each Plenum	Slot Width Each Plenum	Corrugations in Slot	Vane at Source	Inner-Stream Injector Location
IA	1-perforated plate 2 to 10 - 2 slots	2 to 10 - 1/8 in.	No	↓	None
IB	↓	↓	↓	Yes	Opposite plate 2-3
IC	1-11 slots, 2-9 slots 3-7 slots, 4 to 10 - 2 slots	1 to 3-1/16 in. 4 to 10-1/8 in.	1 to 3 - yes 4 to 10 - no	↓	↓
ID	↓	↓	↓	No	↓
IE	↓	↓	↓	↓	Opposite plate 3-4
IF	1-perforated plate 2-9 slots, 3-7 slots 4 to 10 - 2 slots	2+3 - 1/16 in. 4 to 10-1/8 in.	2+3 - yes 4 to 10 - no	↓	↓
IIA	1-perforated plate 2 to 10 - 2 slots	2 to 10-1/8 in.	Yes	No	None
IIB	↓	↓	↓	Yes	Opposite plate 2-3
IIIA	1 perforated plate 2-3 slots, 3-2 slots 4 to 10 - 1 slot	1/8 in.	2+3 - yes 4 to 10 - no	No	Opposite plate 3-4
IIIB	1 perforated plate 2-3 slots, 3-2 slots 4 to 10 - 1 slot, reshaped wall in plenum 9 & 10 region	↓	2 to 10 - yes	↓	↓
IIIC	1-6 slots 2-3 slots, 3-2 slots 4 to 10 - 1 slot, wall shape of IIIB	↓	Yes	↓	↓
IVA	1-perforated plate 2 to 5 - LRC 6 to 10 - 2 slots	2 to 5 - 0.07 in. 6 to 10-1/8 in.	2 to 5 - 0.04 in. open and 0.12 spacer, 6 to 10 - yes	No	Opposite plate 3-4

28

TABLE II

FLOW CONDITIONS FOR OUTER-STREAM INJECTION COMPONENT TESTS

Run No.	Config- uration	Flow Ratio, W_o/W_i	Percent of Total Outer-Stream Flow From Each Plenum, Plenum No. 1 to Plenum No. 10	Chamber Reynolds No. - Re_o $12W_o/(\pi R \mu_o)$
W4	IA	-	1,10,11,11,12,11,11,11,10,11	50,000
W5	IA	-	6,10,11,11,11,11,10,11,10,10	46,000
W6	IA	-	2,6,6,8,10,11,12,14,15,16	46,000
W7	IA	-	3,5,6,7,10,12,12,14,15,16	46,000
W8	IIA	-	2,11,11,11,11,11,11,11,11,11	45,000
W9	IIA	-	5,10,11,10,10,11,11,11,10,11	48,000
W10	IIA	-	3,11,11,11,10,11,11,11,11,11	22,000
W11	IIA	-	2,11,11,11,11,11,11,11,11,11	93,000
W12	IB	33	5,6,7,7,10,11,12,13,14,15	50,000
W13	IB	22	5,6,7,8,9,11,12,13,14,15	52,000
W14	IIB	33	5, 6,6,7,10,11,12,13,14,15	50,000
W15	IIB	21	4,6,7,9,10,11,12,13,14,15	51,000
W16	IC	29	4,7,7,9,9,11,12,13,14,15	53,000
W17	IC	20	10,10,10,10,10,10,10,10,10,10	51,000
W18	IC	33	10,10,9,10,10,10,10,10,10,10	51,000
W19	ID	31	10,10,10,10,10,10,10,10,10,10	51,000
W20	ID	21	9,10,10,10,10,10,9,10,10,10	50,000
W21	ID	22	5,7,8,9,10,11,12,12,13,15	53,000
W22	IIIA	20	10,10,10,10,10,10,10,10,10,10	51,000
W23	IIIB	21	5,6,8,8,9,10,11,12,13,14	54,000
W24	IE	20	10,10,10,10,10,10,10,10,10,10	51,000
W25	IE	21	5,7,8,8,9,10,11,12,13,14	53,000
W26	IE	35	5,7,8,8,9,10,11,12,13,14	53,000
W27	IE	66	5,7,8,8,9,10,11,12,13,14	53,000
W28	IF	20	5,7,8,8,9,11,11,12,13,14	53,000
W29	IF	20	10,10,10,10,10,10,10,10,10,10	51,000
W30	IF	33	10,10,10,10,10,10,10,10,10,10	51,000
W31	IF	35	8,7,8,9,10,11,12,12,13,14	53,000
W32	IVA	22	5,7,8,9,10,11,12,13,13,14	53,000
W33	IVA	35	5,7,8,9,9,11,12,12,14,14	53,000
W34	IVA	20	10,10,10,10,10,10,10,10,10,10	51,000
W35	IIIB	21	10,10,10,10,10,10,10,10,10,10	51,000
W36	IIIB	23	5,7,8,9,10,11,11,12,13,14	53,000
W37	IIIB	21	2,15,13,10,10,10,10,10,10,10	51,000
W38	IIIB	50	10,10,10,10,10,10,10,10,10,10	51,000
W39	IIIB	52	5,7,8,9,10,11,12,13,13,14	53,000
W40	IIIC	53	2,6,8,9,10,11,12,13,14,15	55,000
W41	IIIC	21	2,6,8,9,10,11,12,13,14,15	55,000

$W_O = 0.50$ lb/sec, $W_i = 0.01$ lb/sec, $Z = Z*/L$
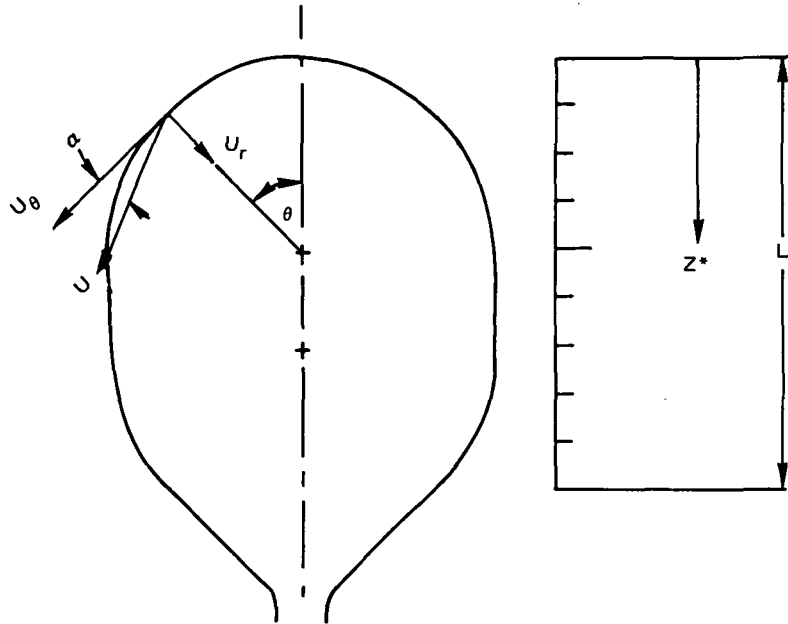
FLOW CONDITION	INJECTION DISTRIBUTION, $dW/dZ = U_r$	INJECTION ANGLE, $a = $ Arc Tan (U_r/U_θ)	
		TOP $4/9^{ths}$	BOTTOM $5/9^{ths}$
IV STANDARD CONDITION	CONSTANT	Arc Tan $(\pi/12/\theta)$	Arc Tan $(1/6)$
V	CONSTANT	Arc Tan $(1/6)$	Arc Tan $(1/6)$
VI	$0.5 + Z$	Arc Tan $(1/6)$	$-$Arc Tan $(1/6)$
VII	$0.5 + Z$	Arc Tan $(\pi/12/\theta)$	Arc Tan $(1/6)$

30

SKETCH OF OPEN CYCLE GASEOUS – CORE NUCLEAR ROCKET ENGINE SHOWING FLUID MECHANICS ASPECTS

FUEL INJECTION AND DEVELOPING FLOW REGION

COAXIAL FLOW REGION

EXHAUST REGION

REFLECTOR–MODERATOR

PROPELLANT REGION

FUEL CONTAINMENT REGION

SUPPLEMENTARY PROPELLANT INJECTION AND WALL COOLING INJECTION

FUEL INJECTION AND VAPORIZATION

UPSTREAM PROPELLANT INJECTION
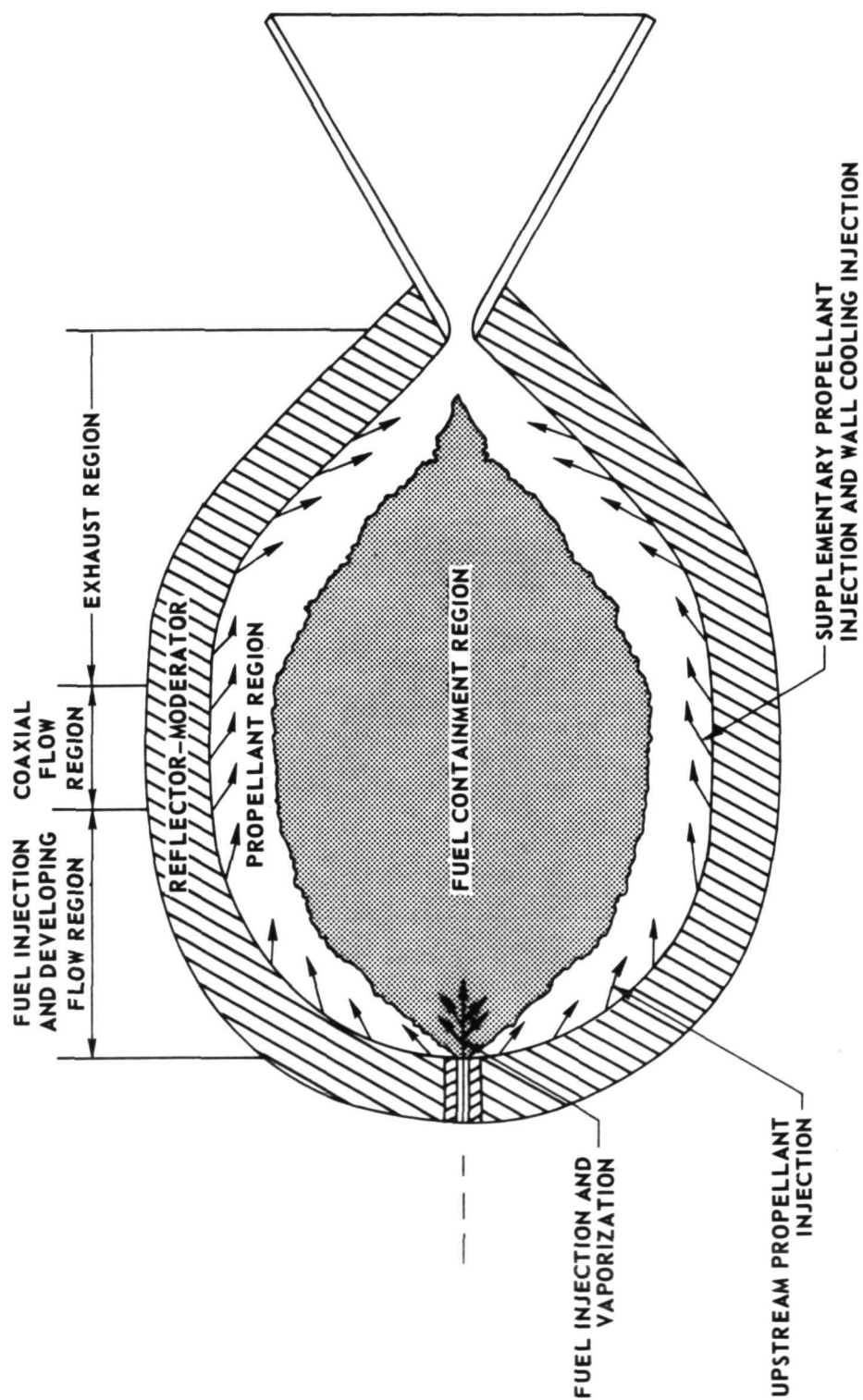
FIGURE 1

31

SCHEMATIC DRAWING OF OUTER-STREAM INJECTION COMPONENT DEVELOPMENT TEST APPRATUS

FOCUSING LENS

BH6
MECURY
LIGHT

1/4 IN. SLIT

CAMERA

FLOWMETERS AND
CONTROL VALVES

TANK

TO DRAIN

PUMP
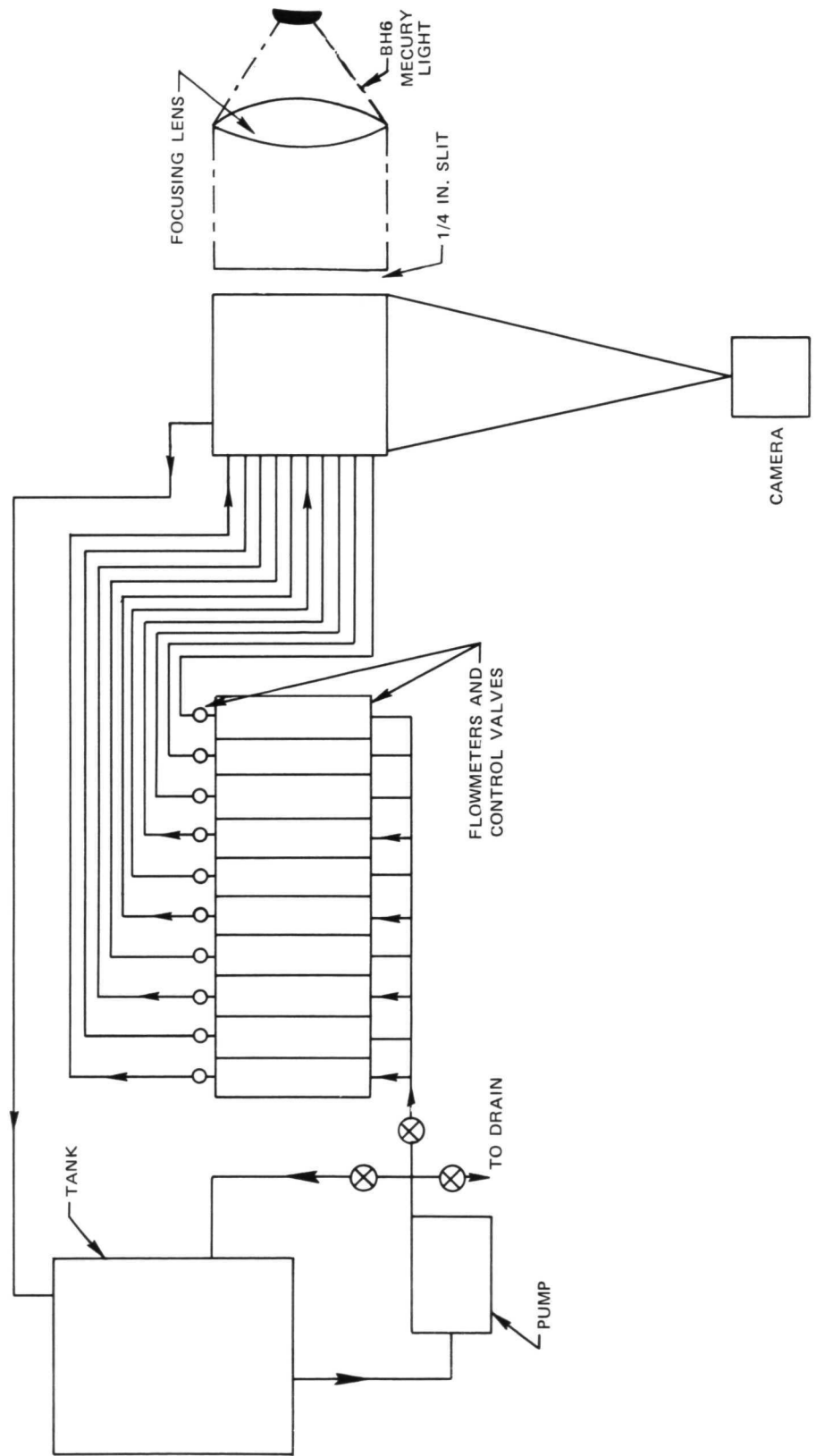
FIGURE 2

**PHOTOGRAPH OF OUTER—STREAM INJECTION COMPONENT
DEVELOPMENT TEST APPARATUS**

FIGURE 3

SKETCH OF OUTER-STREAM INJECTION COMPONENT CONFIGURATIONS I AND II

CONICAL WALL JET GEOMETRY

9.0 IN. (REF.)

PLENUM

1

2

3

4

5

6

7

8

9

10

6 IN. RADIUS

WALL JET

PLENUM WALL

1.5 IN. (TYP)

6 IN. RADIUS

45 DEG.

60°

3 IN.

OPTION -
PERFORATED PLATE
(OR 11 SLOTS)
FORMED OF STAINLESS STEEL
SHEET 0.020 IN. THICK

OPTION -
VANE BETWEEN
INNER-STREAM FLOW
AND OUTER-STREAM FLOW

OPTION -
LOCATION OF 1.0 IN. RADIUS
CERAMIC POROUS HEMISPHERE

OPTION -
NUMBER OF INJECTION
SLOTS FOR PLENUMS
2 AND 3

OPTION
SECTIONS OF HONEYCOMB
OR CORRUGATED METAL
RIBBON INSERTED IN
WALL JET SLOTS

EXHAUST FLOW

FIGURE 4

SKETCH OF OUTER-STREAM INJECTION COMPONENT CONFIGURATION III

COMBINATION ANNULAR AND CONICAL—WALL JET GEOMETRY

FIGURE 5

LEWIS RESEARCH CENTER VANES INSTALLED IN PLENUMS 2 TO 5

(SEE TABLE I FOR NOTE ON CONSTRUCTION)
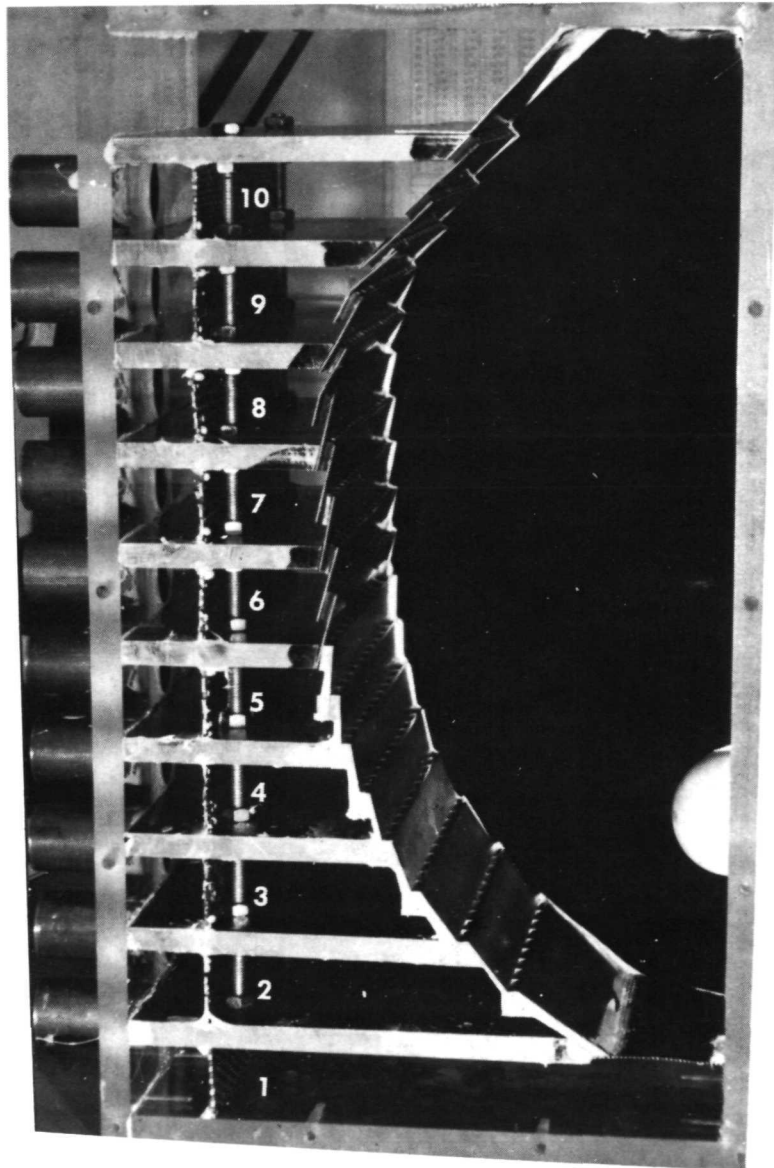
FIGURE 6

EFFECT OF FLOW RATIO AND OUTER–STREAM INJECTION
DISTRIBUTION ON FLOW STRUCTURE WITHIN CONFIGURATION IF

ARROWS INDICATE DYE INJECTION LOCATION
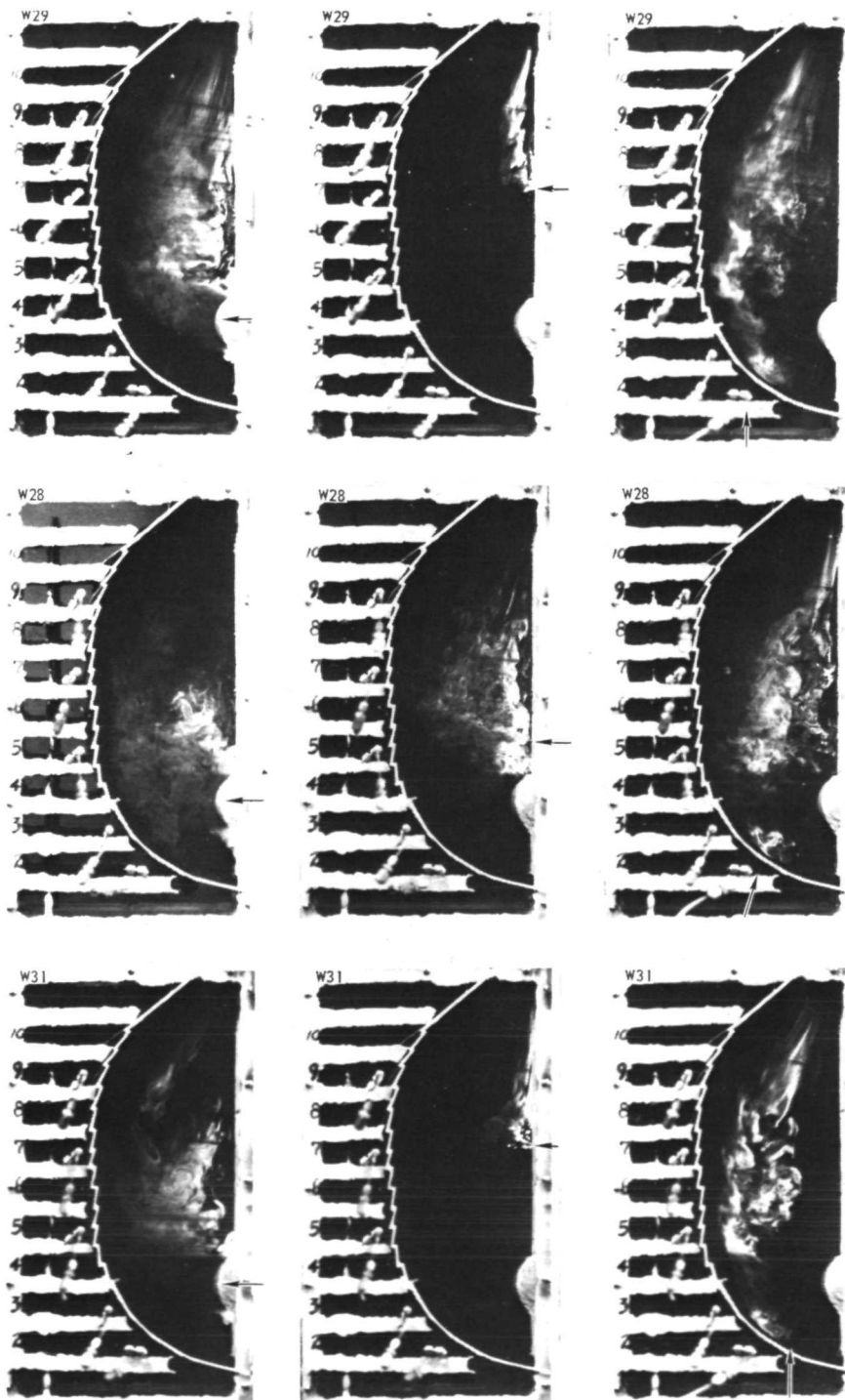
RUN NO. W29

$W_O/W_i = 20$

UNIFORM OUTER–STREAM
FLOW RATE
FROM ALL PLENUMS

RUN NO. W28

$W_O/W_i = 20$

OUTER–STREAM FLOW
RATE INCREASING FROM
UPSTREAM TO EXHAUST
END OF CAVITY

RUN NO. W31

$W_O/W_i = 35$

OUTER–STREAM FLOW
RATE INCREASING FROM
UPSTREAM TO EXHAUST
END OF CAVITY

FIGURE 7

37

EFFECT OF FLOW RATIO AND OUTER—STREAM INJECTION
DISTRIBUTION ON FLOW STRUCTURE WITHIN CONFIGURATION ⅢB

ARROWS INDICATE DYE INJECTION LOCATION
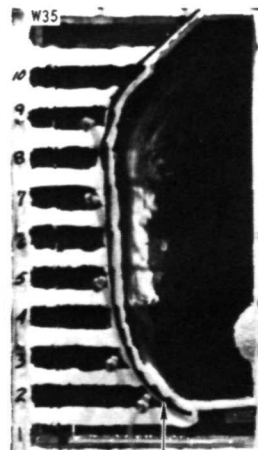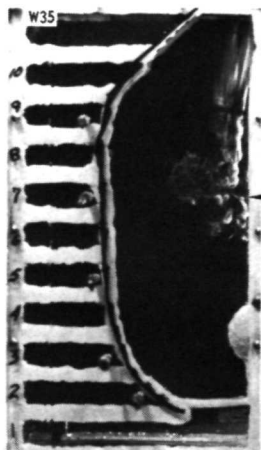
RUN NO. W35

$W_O/W_i = 21$

UNIFORM OUTER—STREAM

FLOW RATE

FROM ALL PLENUMS
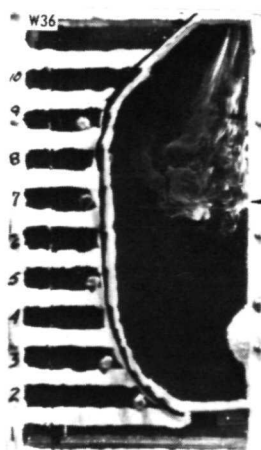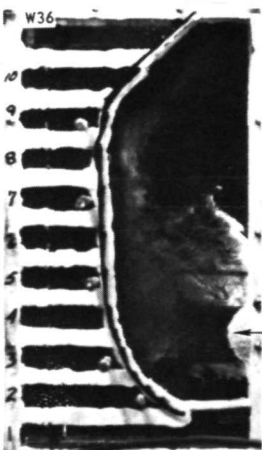
RUN NO. W36

$W_O/W_i = 23$

OUTER—STREAM FLOW

RATE INCREASING FROM

UPSTREAM TO EXHAUST
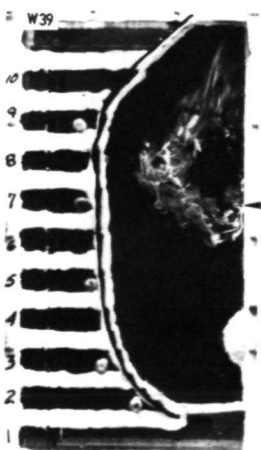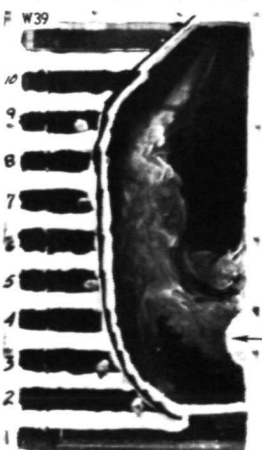
END OF CAVITY

RUN NO. W39

$W_O/W_i = 52$

OUTER—STREAM FLOW

RATE INCREASING FROM

UPSTREAM TO EXHAUST

END OF CAVITY

FIGURE 8

EFFECT OF FLOW RATIO AND OUTER—STREAM INJECTION
DISTRIBUTION ON FLOW STRUCTURE WITHIN CONFIGURATION IVA

ARROWS INDICATE DYE INJECTION LOCATION
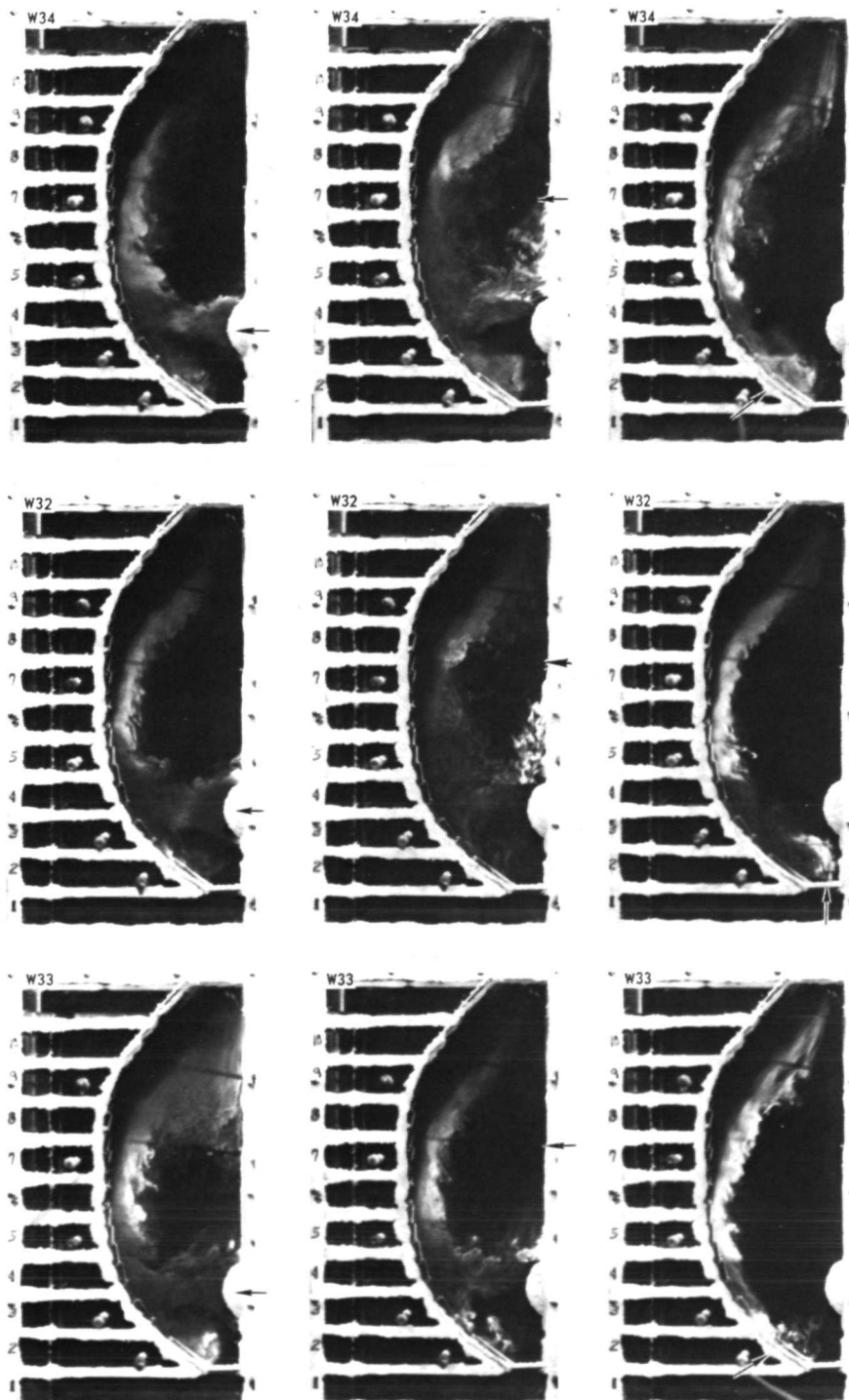
RUN NO. W34

$W_O/W_i = 20$

UNIFORM OUTER—STREAM

FLOW RATE

FROM ALL PLENUMS

RUN NO. W32

$W_O/W_i = 22$

OUTER—STREAM FLOW

RATE INCREASING FROM

UPSTREAM TO EXHAUST

END OF CAVITY

RUN NO. W33

$W_O/W_i = 35$

OUTER—STREAM FLOW

RATE INCREASING FROM

UPSTREAM TO EXHAUST

END OF CAVITY

FIGURE 9

EFFECT OF FLOW RATIO AND OUTER–STREAM INJECTION
DISTRIBUTION ON FLOW STRUCTURE WITHIN CONFIGURATION IE

ARROWS INDICATE DYE INJECTION LOCATION

RUN NO. W24

$W_O/W_i = 20$

UNIFORM OUTER–STREAM

FLOW RATE

FROM ALL PLENUMS
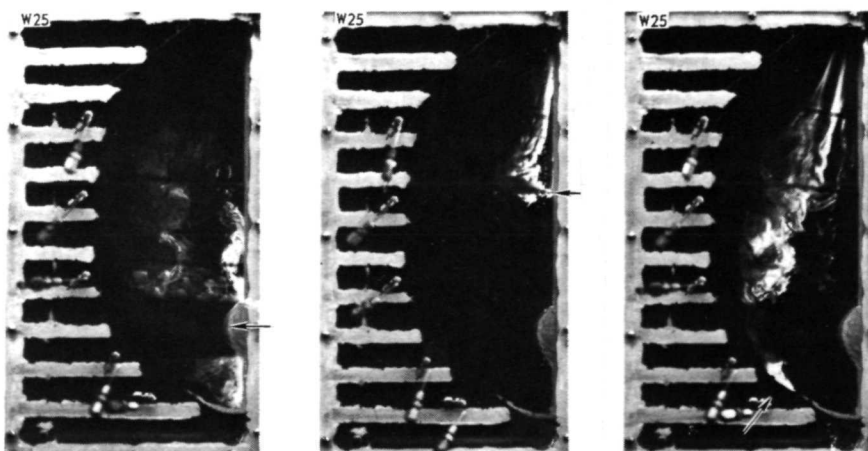
RUN NO. W25

$W_O/W_i = 21$

OUTER–STREAM FLOW

RATE INCREASING FROM

UPSTREAM TO EXHAUST
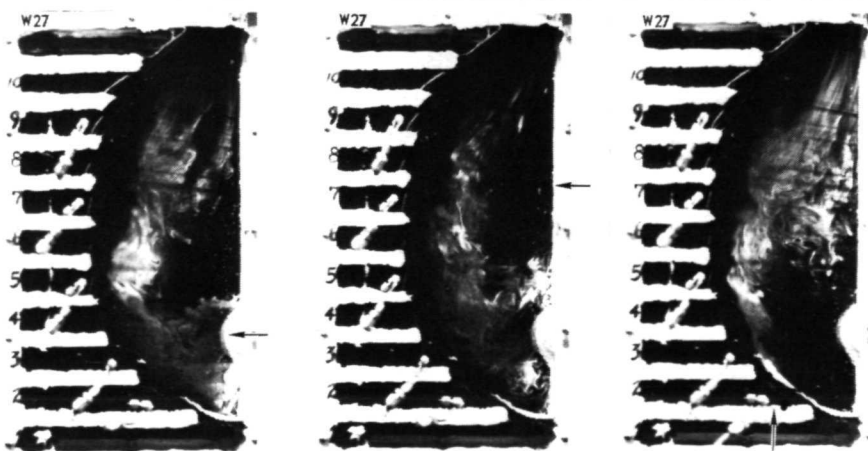
END OF CAVITY

RUN NO. W27

$W_O/W_i = 66$

OUTER–STREAM FLOW

RATE INCREASING FROM

UPSTREAM TO EXHAUST

END OF CAVITY

FIGURE 10

40

EFFECT OF FLOW RATIO ON FLOW STRUCTURE WITHIN CONFIGURATION IIIC

ARROWS INDICATE DYE INJECTION LOCATION
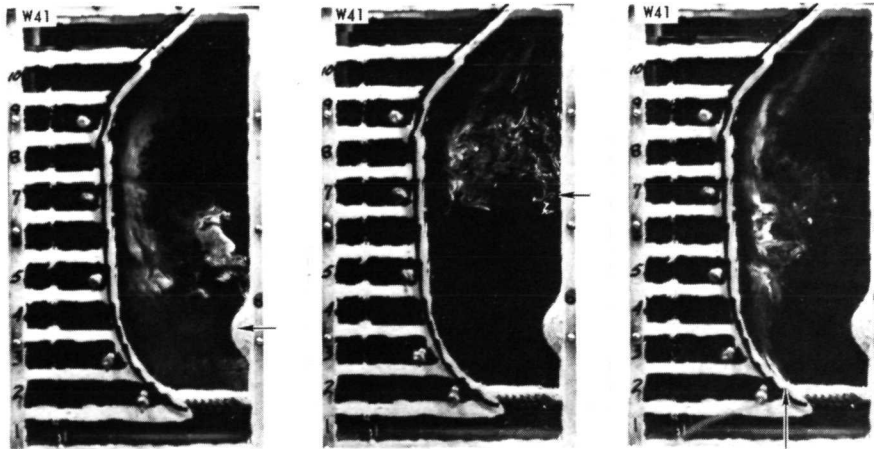
RUN NO.W41
$W_O/W_i = 21$
OUTER—STREAM FLOW
RATE INCREASING FROM
UPSTREAM TO EXHAUST
END OF CAVITY
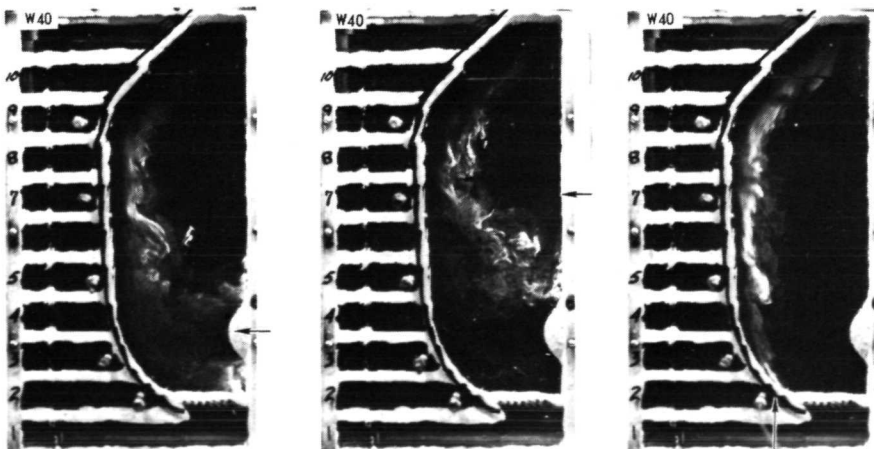
RUN NO.W 40
$W_O/W_i = 53$
OUTER—STREAM FLOW
RATE INCREASING FROM
UPSTREAM TO EXHAUST
END OF CAVITY

FIGURE 11

EFFECT OF INNER–STREAM INJECTOR LOCATION
ON FLOW STRUCTURE WITHIN CONFIGURATION

OUTER–STREAM FLOW RATE INCREASING FROM UPSTREAM TO EXHAUST END OF CAVITY
ARROWS INDICATE DYE INJECTION LOCATION
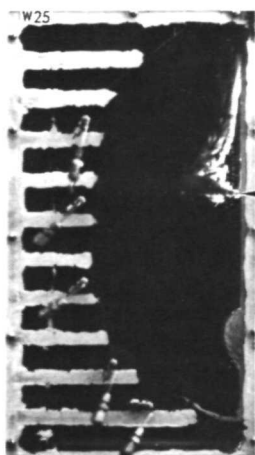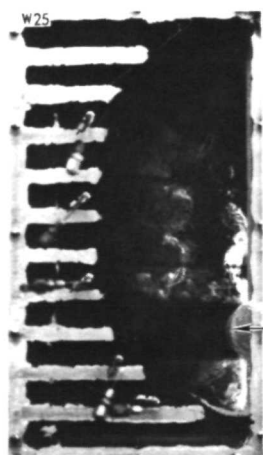
RUN NO. W25

$W_O/W_i = 21$

CONFIGURATION I E

INNER–STREAM
INJECTOR OPPOSITE
PLATE 3–4
NO VANE INSTALLED

RUN NO. W21

$W_O/W_i = 22$

CONFIGURATION I D

INNER–STREAM
INJECTOR OPPOSITE
PLATE 2–3
NO VANE INSTALLED
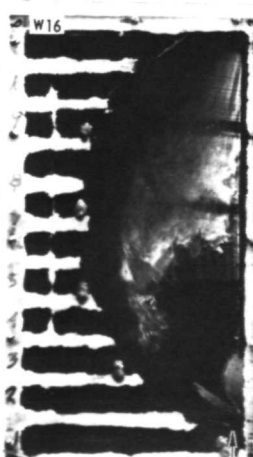
RUN NO. W16

$W_O/W_i = 28$

CONFIGURATION I C

INNER–STREAM
INJECTOR OPPOSITE
PLATE 2–3
VANE INSTALLED

FIGURE 12

SKETCH SHOWING BOUNDARY CONDITIONS USED FOR SPHERICAL CAVITY CALCULATIONS

$Z = Z*/L$
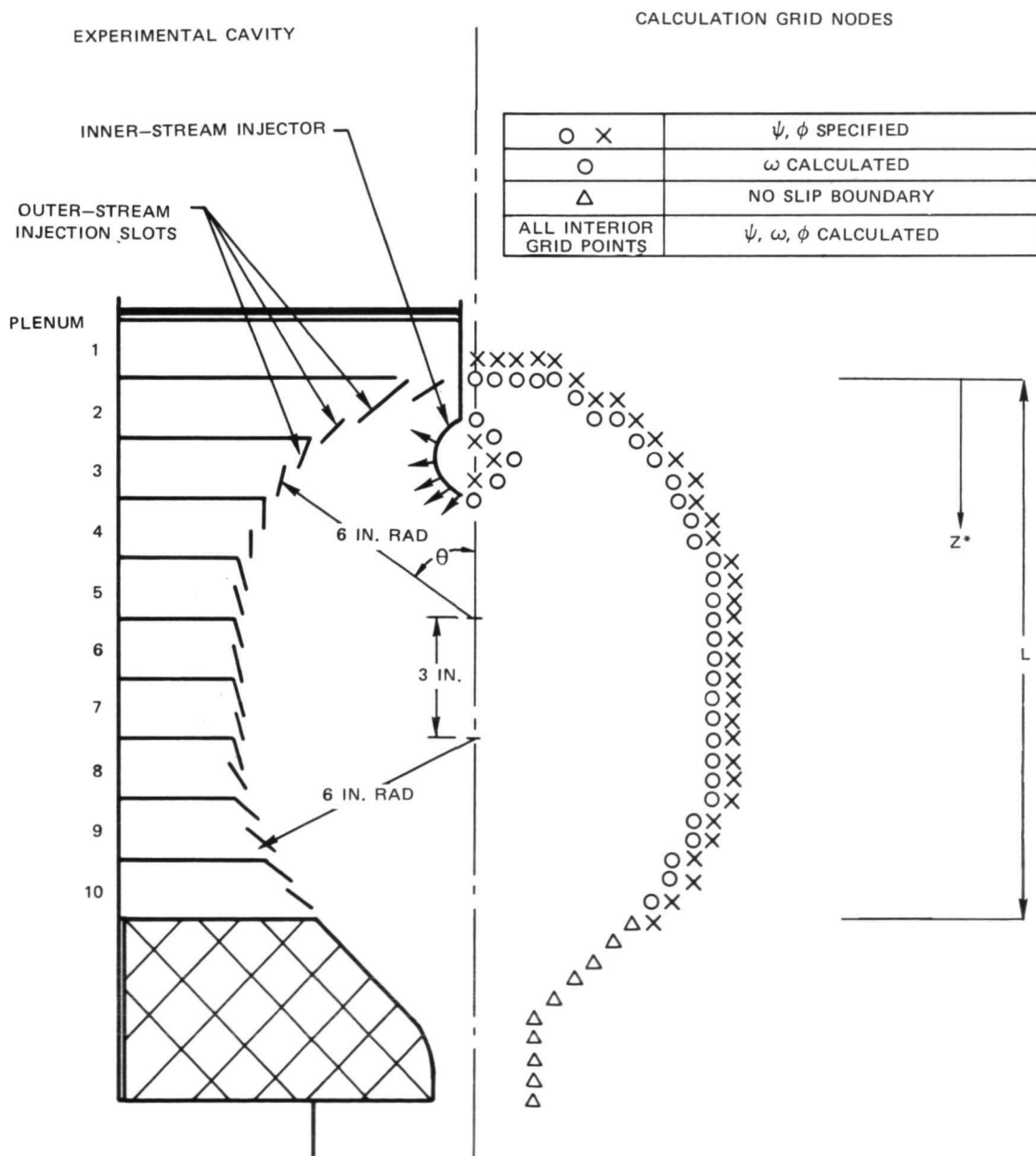
FIGURE 13

43

COMPUTED STREAMLINE DISTRIBUTION FOR STANDARD CONDITION

OUTER—STREAM INJECTION DISTRIBUTION — CASE IV (SEE TABLE III)

KINEMATIC VISCOSITY — $\nu = 0.1$ ft^2/sec

GRAVITY = 1 DOWNWARD (32 ft/sec^2)

SCHMIDT NUMBER = $\nu/D = 1.0$

DENSITY RATIO — $\rho_i/\rho_o = 4.7$

U$_r$ — CONSTANT, a — VARIES

○ □	ψ, ϕ SPECIFIED
○	ω CALCULATED
△	NO SLIP BOUNDARY
ALL INTERIOR GRID POINTS	ψ, ω, ϕ CALCULATED

LINE NUMBER	1	2	3	4	5	6	7	8	9
PERCENT OF TOTAL FLOW	100	75	50	25	10	5	2	1	0
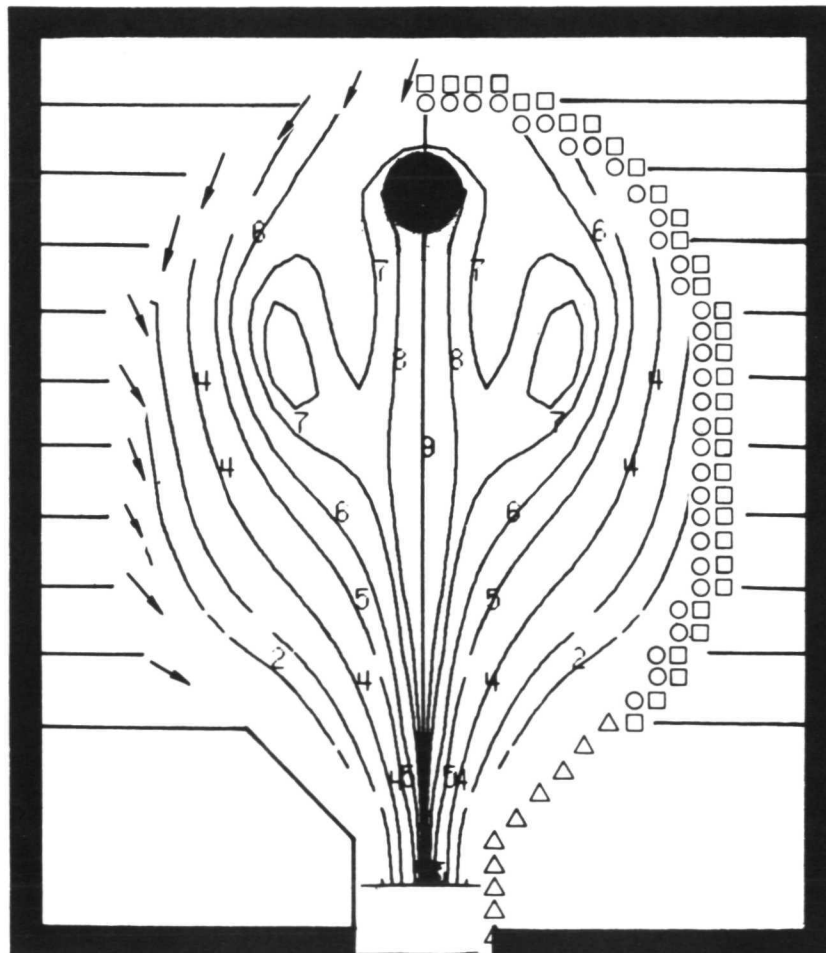
FIGURE 14

44

COMPUTED CONCENTRATION DISTRIBUTION FOR STANDARD CONDITION

OUTER–STREAM INJECTION DISTRIBUTION – CASE IV (SEE TABLE III)

KINEMATIC VISCOSITY – $v = 0.1$ ft^2/sec

GRAVITY = 1 DOWNWARD (32 ft/sec^2)

SCHMIDT NUMBER = v/D = 1.0

DENSITY RATIO – ρ_i/ρ_o = 4.7

U_r – CONSTANT, a – VARIES

LINE NUMBER	1	2	3	4	5	6	7	8	9	10	11	12
P_i/P	0.90	0.70	0.50	0.30	0.20	0.10	0.05	0.02	0.01	0.005	0.002	0.001
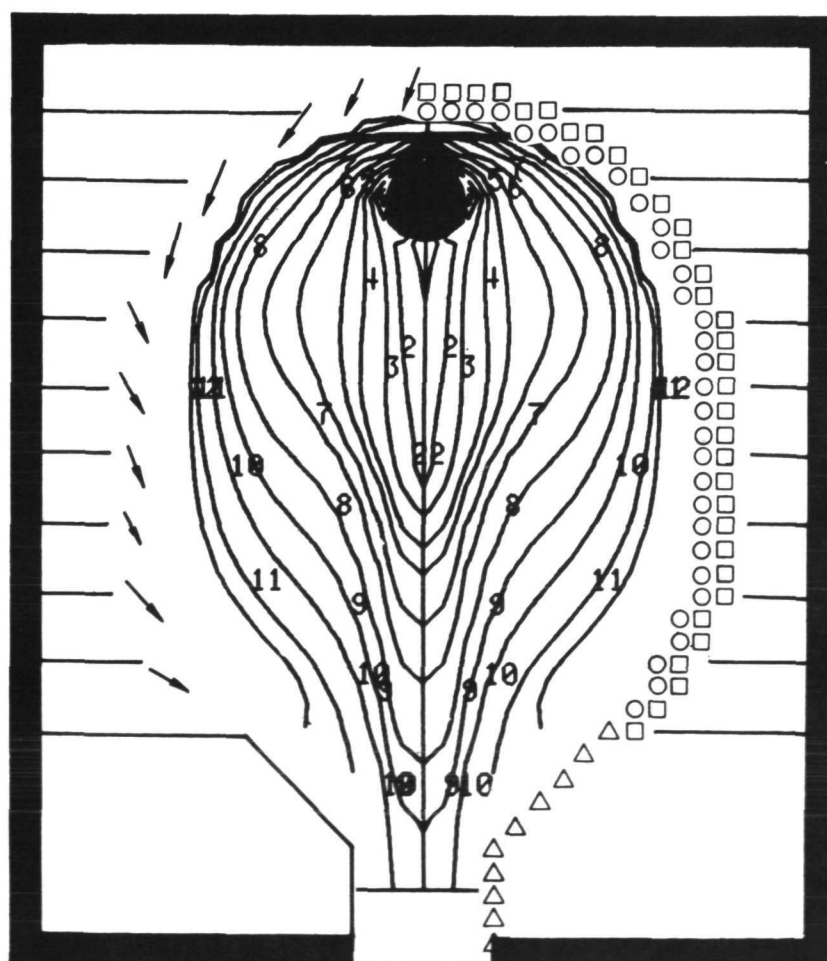
FIGURE 15

45

COMPUTED EFFECT OF OUTER–STREAM INJECTION DISTRIBUTION
ON STREAMLINE DISTRIBUTION

SEE TABLE III FOR OUTER–STREAM INJECTION DISTRIBUTIONS

LINE NUMBER	1	2	3	4	5	6	7	8	9	10	11	12	13
PERCENT OF TOTAL FLOW	100	75	50	25	10	5	2	1	0	−1	−2	−5	−10

STANDARD CONDITION
CASE IV
U_r – CONSTANT, a – VARIES
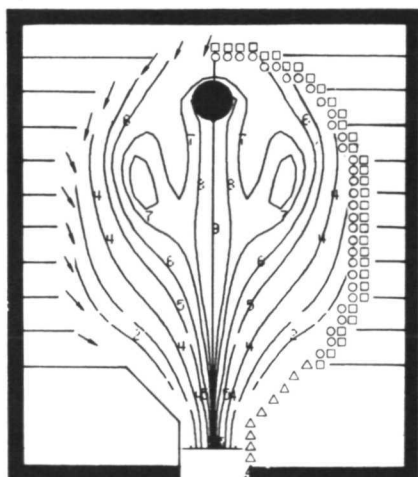
CASE V
U_r – CONSTANT, a – CONSTANT
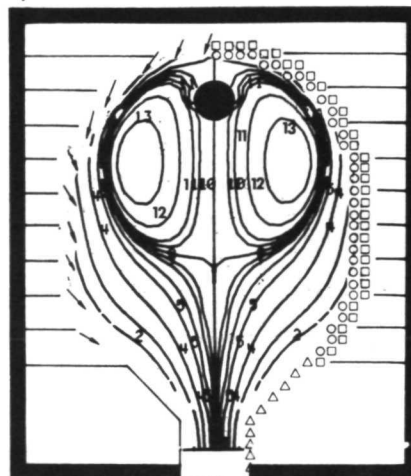
CASE VII
U_r – VARIES, a – VARIES
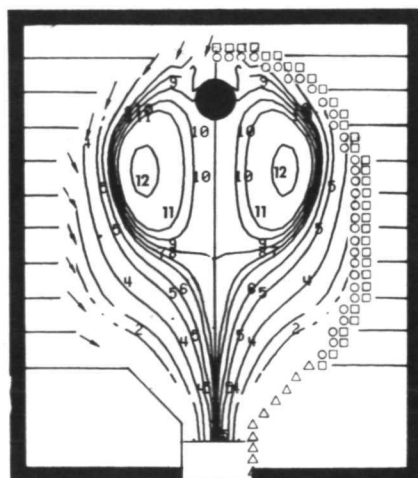
CASE VIII
U_r – VARIES, a – CONSTANT
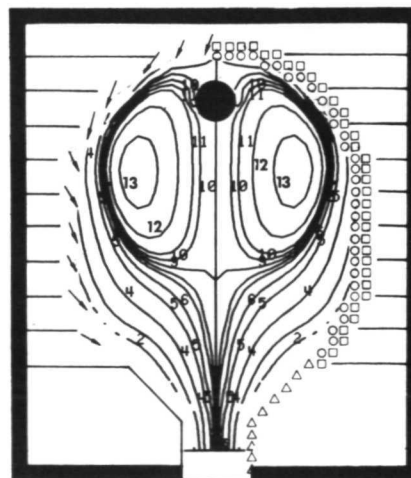
FIGURE 16

46

COMPUTED EFFECT OF OUTER—STREAM INJECTION DISTRIBUTION ON CONCENTRATION DISTRIBUTION

SEE TABLE III FOR OUTER—STREAM INJECTION DISTRIBUTIONS

LINE NUMBER	1	2	3	4	5	6	7	8	9	10	11	12
P_i/P	0.90	0.70	0.50	0.30	0.20	0.10	0.05	0.02	0.01	0.005	0.002	0.001

STANDARD CONDITION
CASE IV
$\overline{P}_i/P = 0.040$
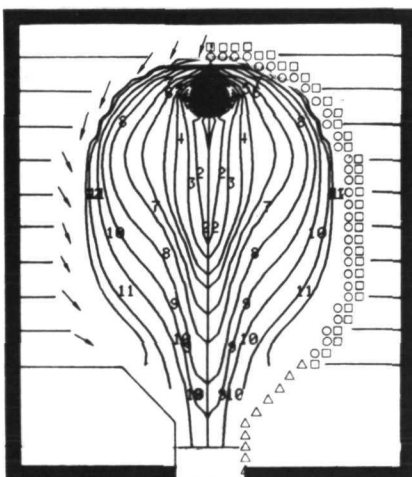
CASE V
$\overline{P}_i/P = 0.013$
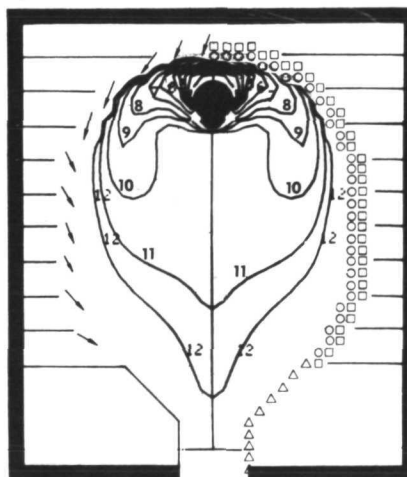
CASE VII
$\overline{P}_i/P = 0.021$
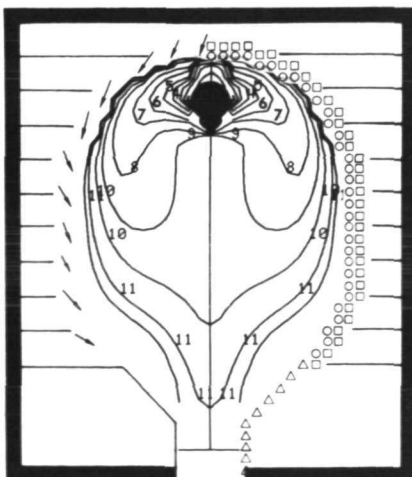
CASE VI
$\overline{P}_i/P = 0.014$
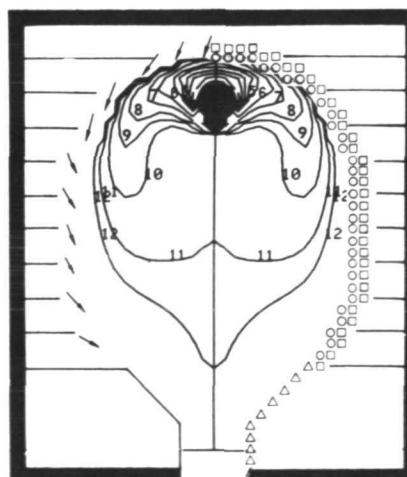
FIGURE 17

47

COMPUTED EFFECT OF KINEMATIC VISCOSITY ON STREAMLINE DISTRIBUTION

LINE NUMBER	1	2	3	4	5	6	7	8	9	10	11
PERCENT OF TOTAL FLOW	100	75	50	25	10	5	2	1	0	−1	−2

$\nu = 1.0$ ft^2/sec
$Re_{s,t} = 10$
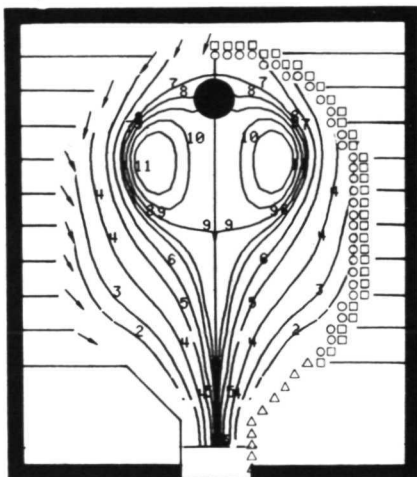
STANDARD CONDITION
$\nu = 0.1$ ft^2/sec
$Re_{s,t} = 100$
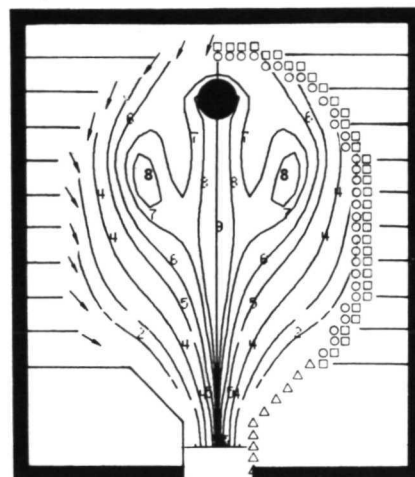
$\nu = 0.03$ ft^2/sec
$Re_{s,t} = 333$
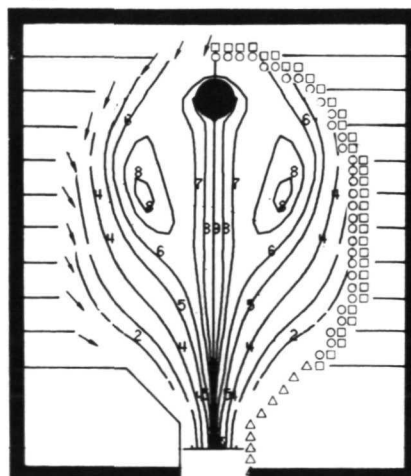
FIGURE 18

48

COMPUTED EFFECT OF KINEMATIC VISCOSITY ON CONCENTRATION DISTRIBUTION

LINE NUMBER	1	2	3	4	5	6	7	8	9	10	11	12
P_i/P	0.90	0.70	0.50	0.30	0.20	0.10	0.05	0.02	0.01	0.005	0.002	0.001

$\nu = 1.0 \ \text{ft}^2/\text{sec}$
$\bar{P}_i/P = 0.017$
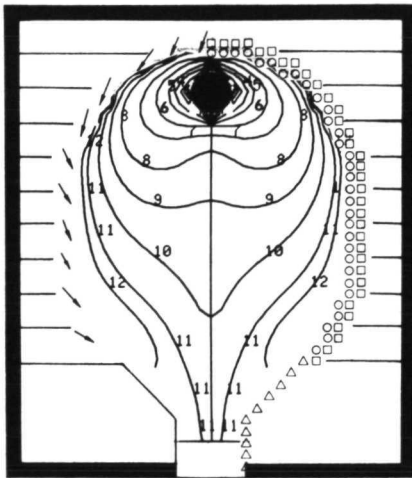
STANDARD CONDITION
$\nu = 0.1 \ \text{ft}^2/\text{sec}$
$\bar{P}_i/P = 0.040$
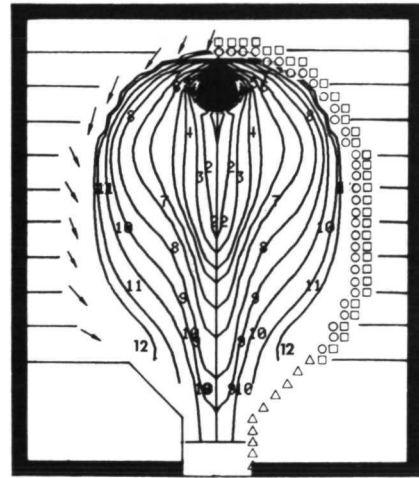
$\nu = 0.03 \ \text{ft}^2/\text{sec}$
$\bar{P}_i/P = 0.026$
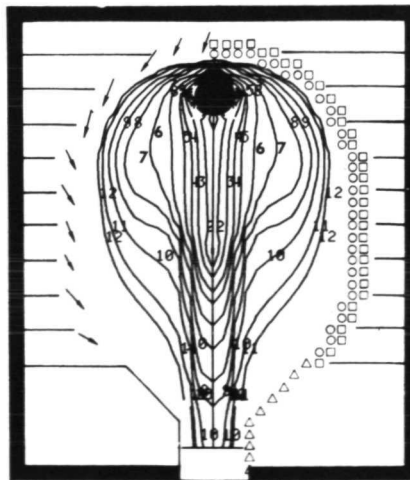
FIGURE 19

49

COMPUTED EFFECT OF GRAVITY ON STREAMLINE DISTRIBUTION

BUOYANCY PARAMETER , $B = [(\rho_i - \rho_o) gD/(\rho_i U_i^2)]^{\frac{1}{2}}$

LINE NUMBER	1	2	3	4	5	6	7	8	9
PERCENT OF TOTAL FLOW	100	75	50	25	10	5	2	1	0

GRAVITY = −1 (UPWARD)
BUOYANCY NO., B = −15
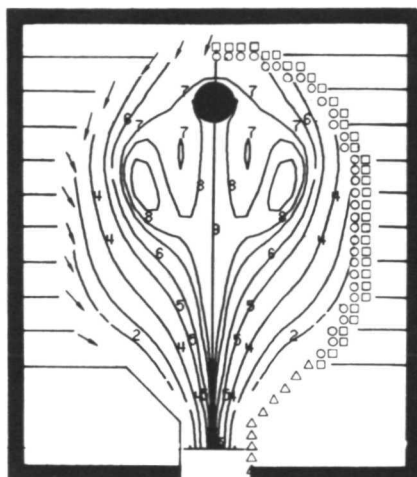
GRAVITY = 0
BUOYANCY NO., B = 0
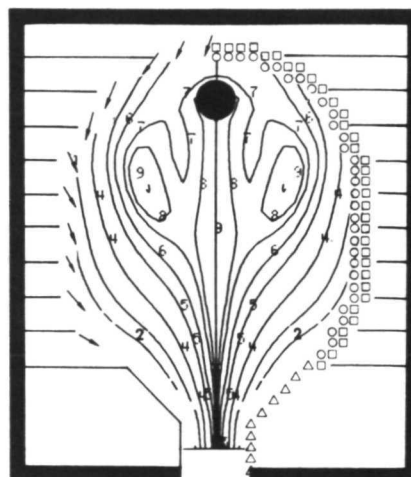
STANDARD CONDITION
GRAVITY = 1 (DOWNWARD)
BUOYANCY NO., B = 15
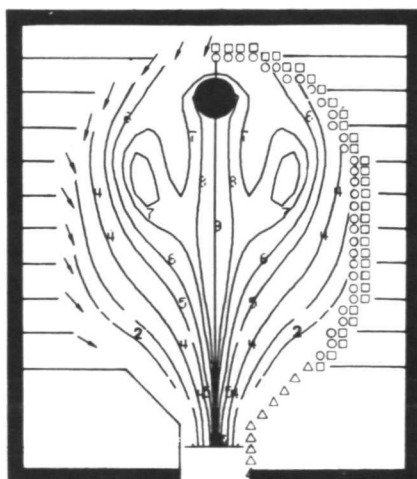
GRAVITY = 100 (DOWNWARD)
BUOYANCY NO., B = 150
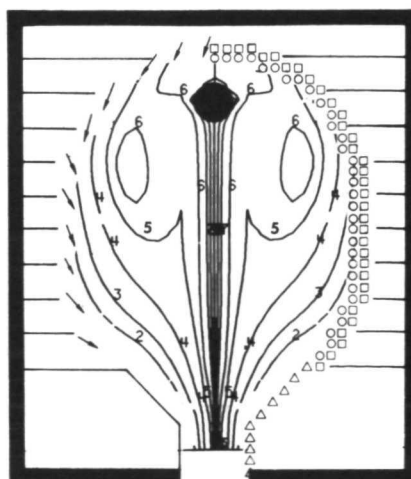
FIGURE 20

COMPUTED EFFECT OF GRAVITY ON CONCENTRATION DISTRIBUTION

BUOYANCY PARAMETER, $B = [(\rho_i - \rho_o) gD/(\rho_i U_i^2)]^{1/2}$

LINE NUMBER	1	2	3	4	5	6	7	8	9	10	11	12
P_i/P	0.90	0.70	0.50	0.30	0.20	0.10	0.05	0.02	0.01	0.005	0.002	0.001

GRAVITY = −1 (UPWARD)
$\bar{P}_i/P$ = 0.045
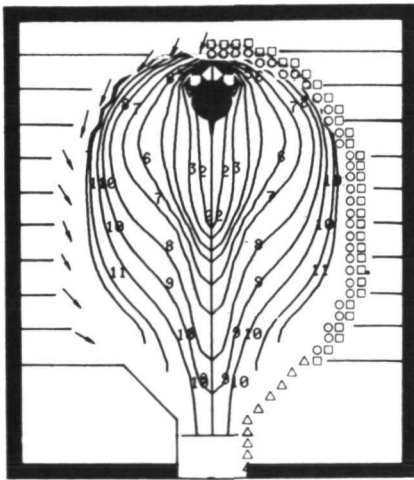
GRAVITY = 0
$\bar{P}_i/P$ = 0.043
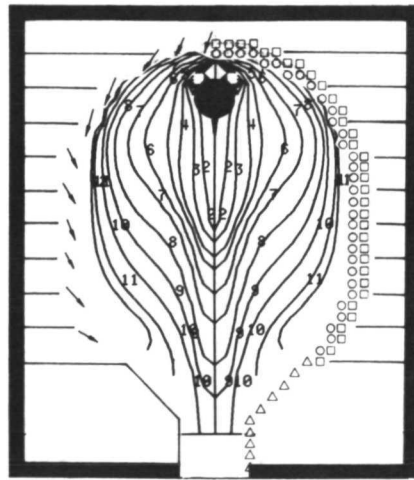
STANDARD CONDITION
GRAVITY = 1 (DOWNWARD)
$\bar{P}_i/P$ = 0.040
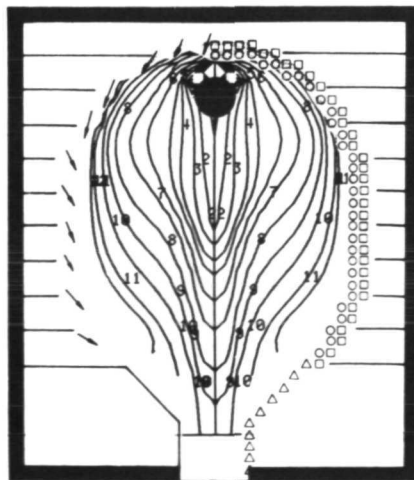
GRAVITY = 100 (DOWNWARD)
$\bar{P}_i/P$ = 0.011
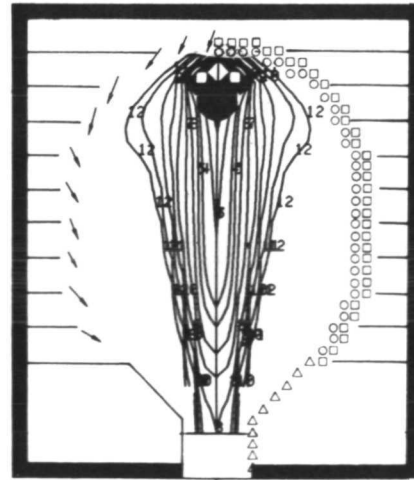
FIGURE 21

COMPUTED EFFECT OF DENSITY RATIO ON STREAMLINE
AND CONCENTRATION DISTRIBUTIONS

LINE NUMBER	1	2	3	4	5	6	7	8	9	10	11	12
P_i/P	0.90	0.70	0.50	0.30	0.20	0.10	0.05	0.02	0.01	0.005	0.002	0.001
PERCENT OF TOTAL FLOW	100	75	50	25	10	5	2	1	0			

STREAMLINES

STANDARD CONDITION
$\rho_i/\rho_o = 4.7$ $\rho_i/\rho_o = 1.0$
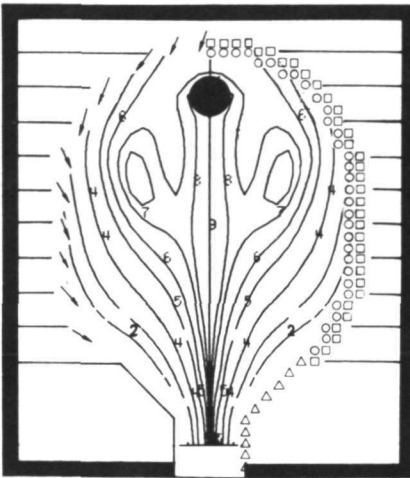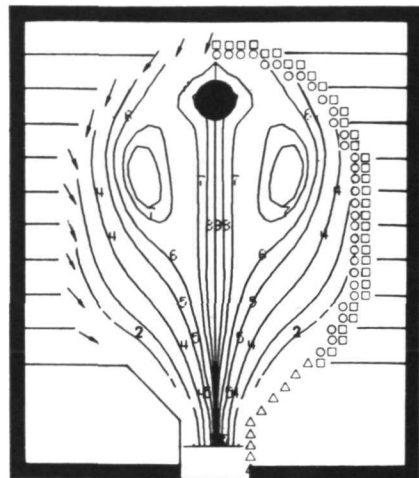
CONCENTRATION PROFILES
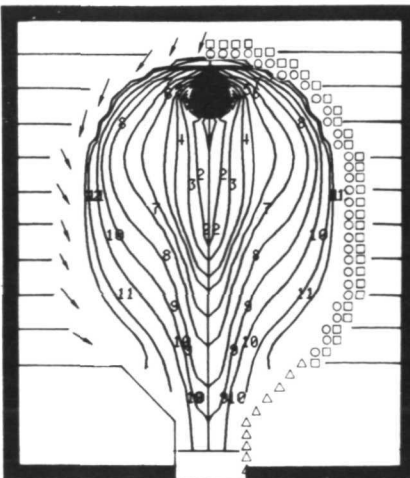
$\rho_i/\rho_o = 4.7$ $\rho_i/\rho_o = 1.0$
$\overline{P}_i/P = 0.040$ $\overline{P}_i/P = 0.053$
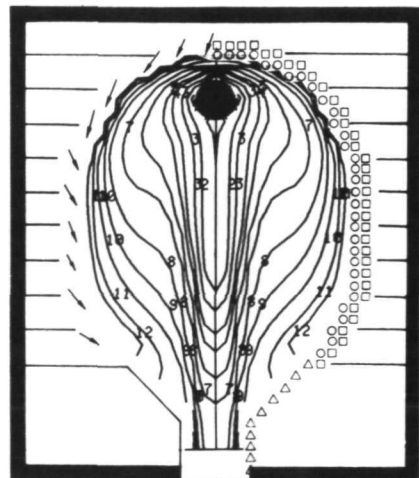
FIGURE 22

COMPUTED EFFECT OF SCHMIDT NUMBER ON STREAMLINE
AND CONCENTRATION DISTRIBUTIONS

SCHMIDT NUMBER = ν/D

LINE NUMBER	1	2	3	4	5	6	7	8	9	10	11	12
P_i/P	0.90	0.70	0.50	0.30	0.20	0.10	0.05	0.02	0.01	0.005	0.002	0.001
PERCENT OF TOTAL FLOW	100	75	50	25	10	5	2	1	0			

STREAMLINES

STANDARD CONDITION
SCHMIDT NO. = 1.0
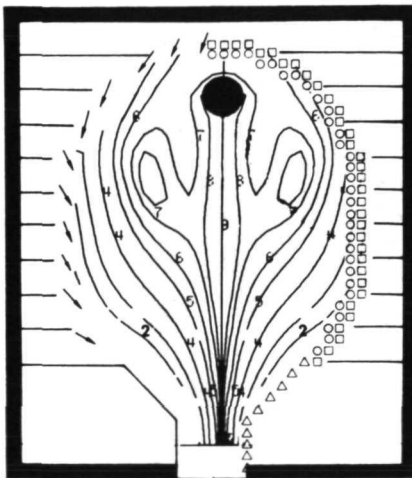
SCHMIDT NO. = 10.0
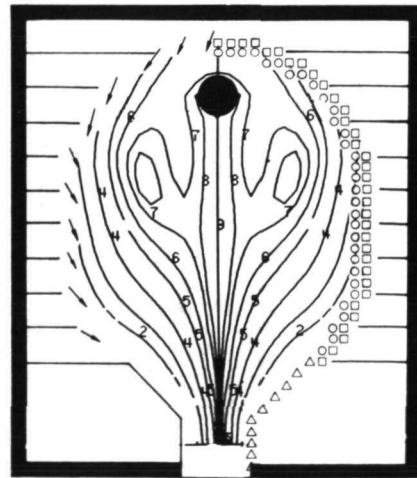
CONCENTRATION PROFILES

SCHMIDT NO. = 1.0
$\bar{P}_i/P = 0.040$
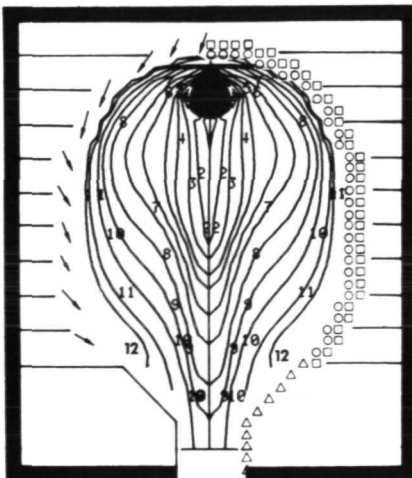
SCHMIDT NO. = 10.0
$\bar{P}_i/P = 0.037$
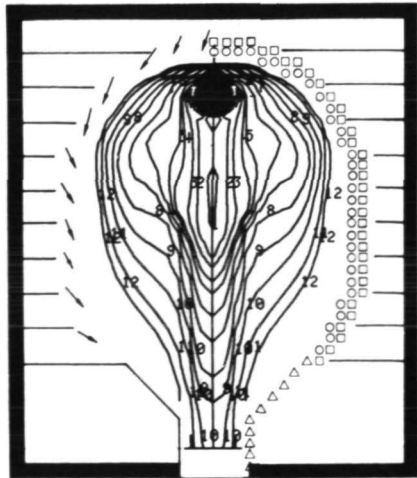
FIGURE 23

PHOTOGRAPH OF SPHERICAL CAVITY TEST APPARATUS
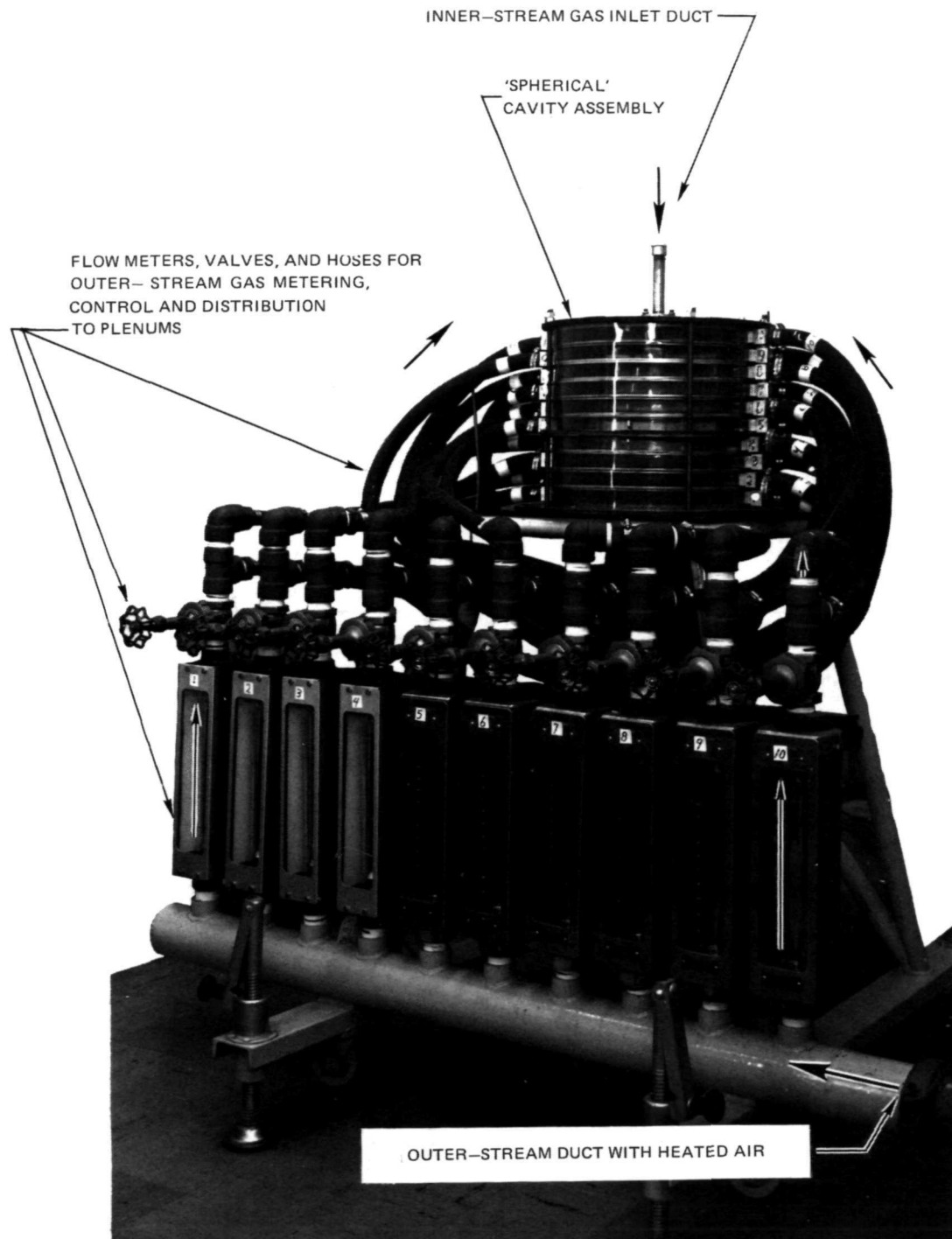
FIGURE 24

PHOTOGRAPH OF SPHERICAL CAVITY ASSEMBLED
WITHOUT INJECTION CONFIGURATIONS

SECTIONS ABOVE AND BELOW THE DOUBLE PLATE NEAR CENTER ARE CYLINDRICAL SECTIONS.
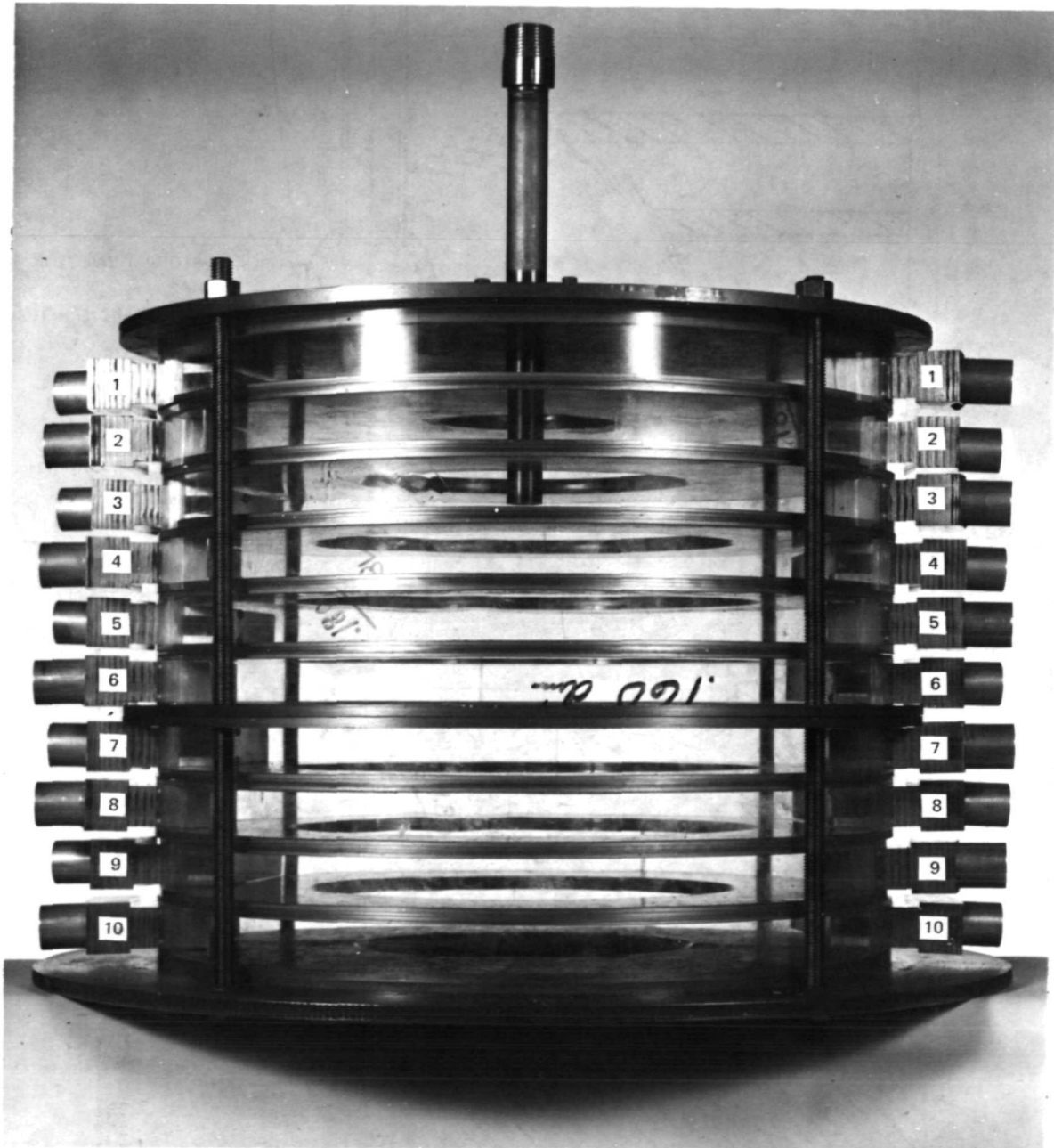
FIGURE 25

CROSS – SECTIONAL SKETCH OF SPHERICAL CAVITY VB

COMBINATION WALL JET CONFIGURATION

9.0 IN. RADIUS (REF.)

PLENUM

INNER-STREAM INJECTOR:
2 IN. DIA
POROUS CERAMIC SPHERE

LEXAN SHEET

1/8 IN. SLOT
WITH 0.003 IN. THICK
CORRUGATED RIBBON

AXIS OF SYMMETRY

45 DEG.

EXHAUST FLOW
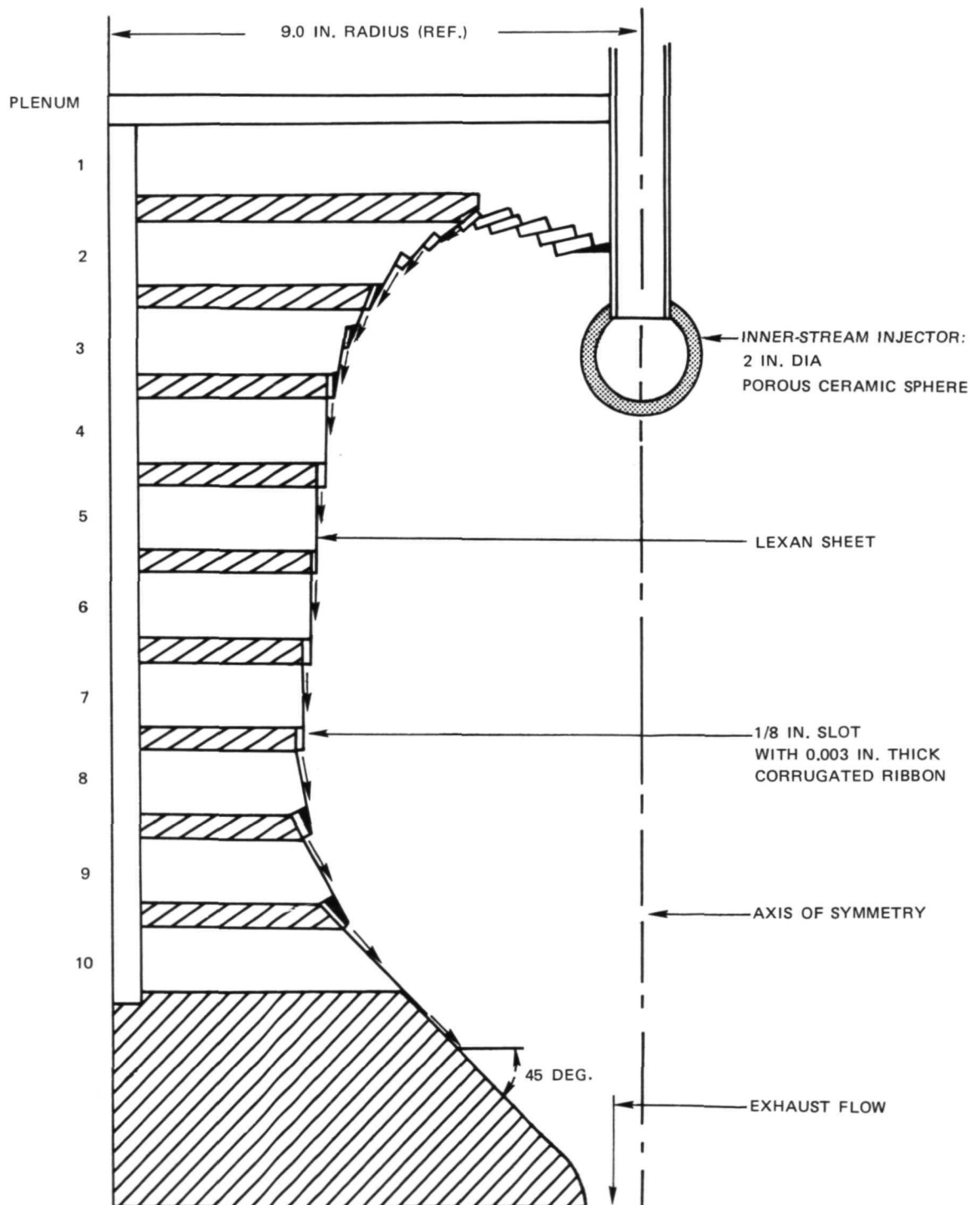
FIGURE 26

SCHEMATIC OF OPTICAL SYSTEM FOR FLOW VISUALIZATION PHOTOGRAPHY

TOP VIEW
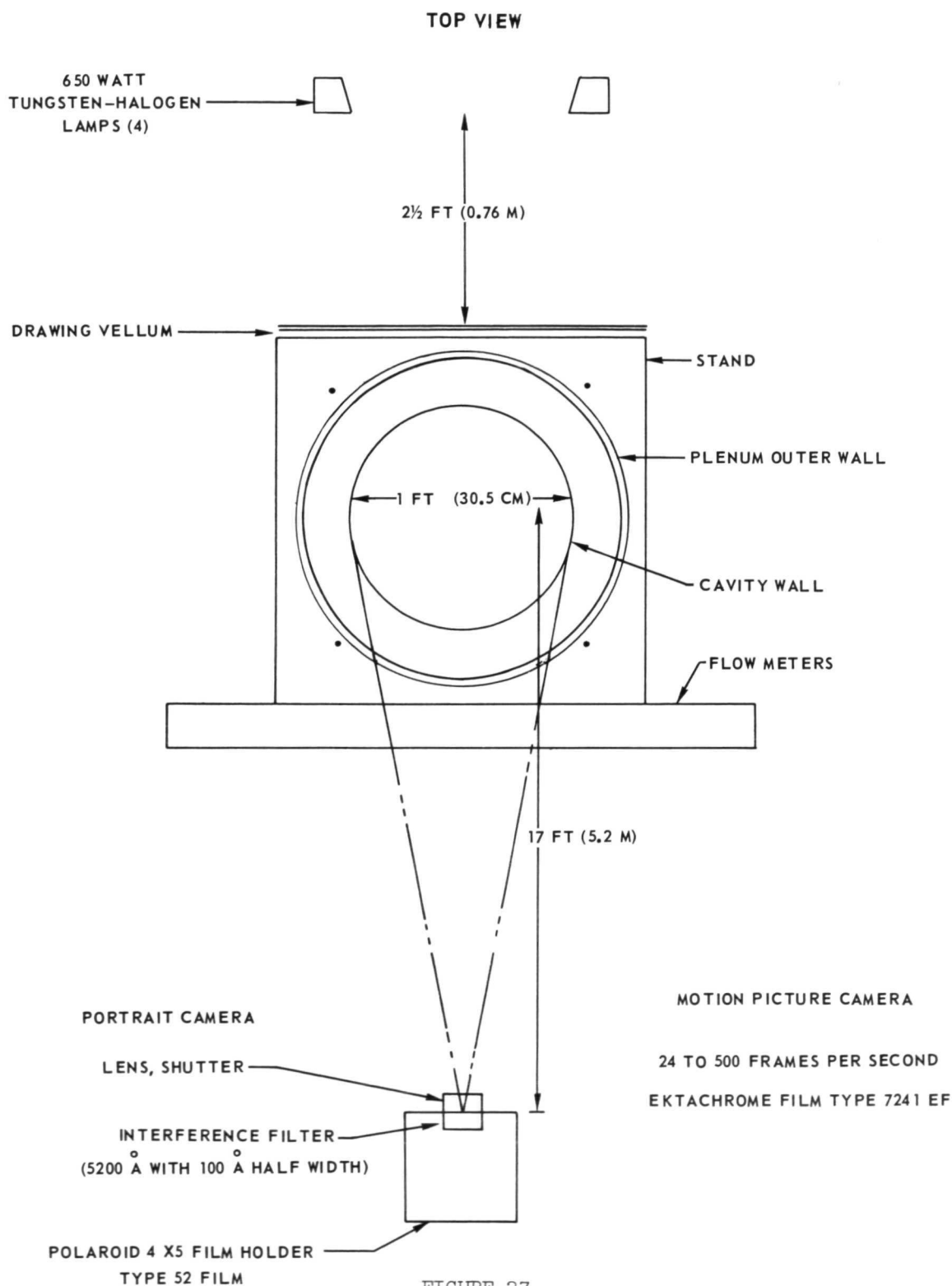
FIGURE 27

PHOTOGRAPH OF TIME—OF—FLIGHT MASS SPECTROMETER AND SPHERICAL CAVITY TEST APPARATUS
USED TO OBTAIN INNER GAS CONCENTRATION DISTRIBUTION
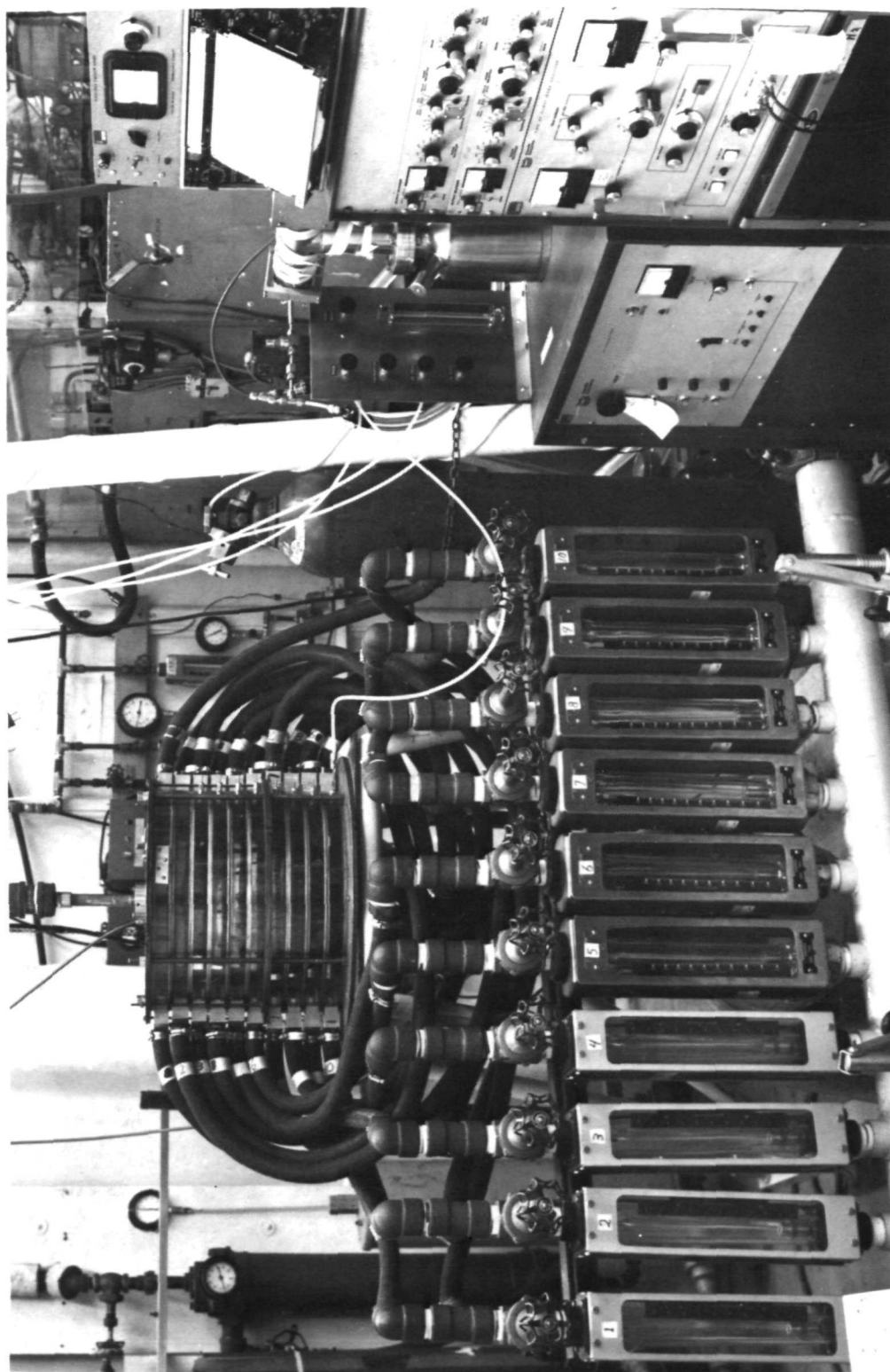
FIGURE 28

DISTRIBUTION OF OUTER—STREAM FLOW THROUGH SPHERICAL CAVITY PLENUMS

COMBINATION WALL JET CAVITY
$W_O \approx 0.5$ LB/SEC (0.23 K_g /SEC)

SYMBOL	──O──	──△──	┅□┅	⋯◇⋯
RUN NO.	202–20.4	205	206	207
W_O/W_i		25	50	100
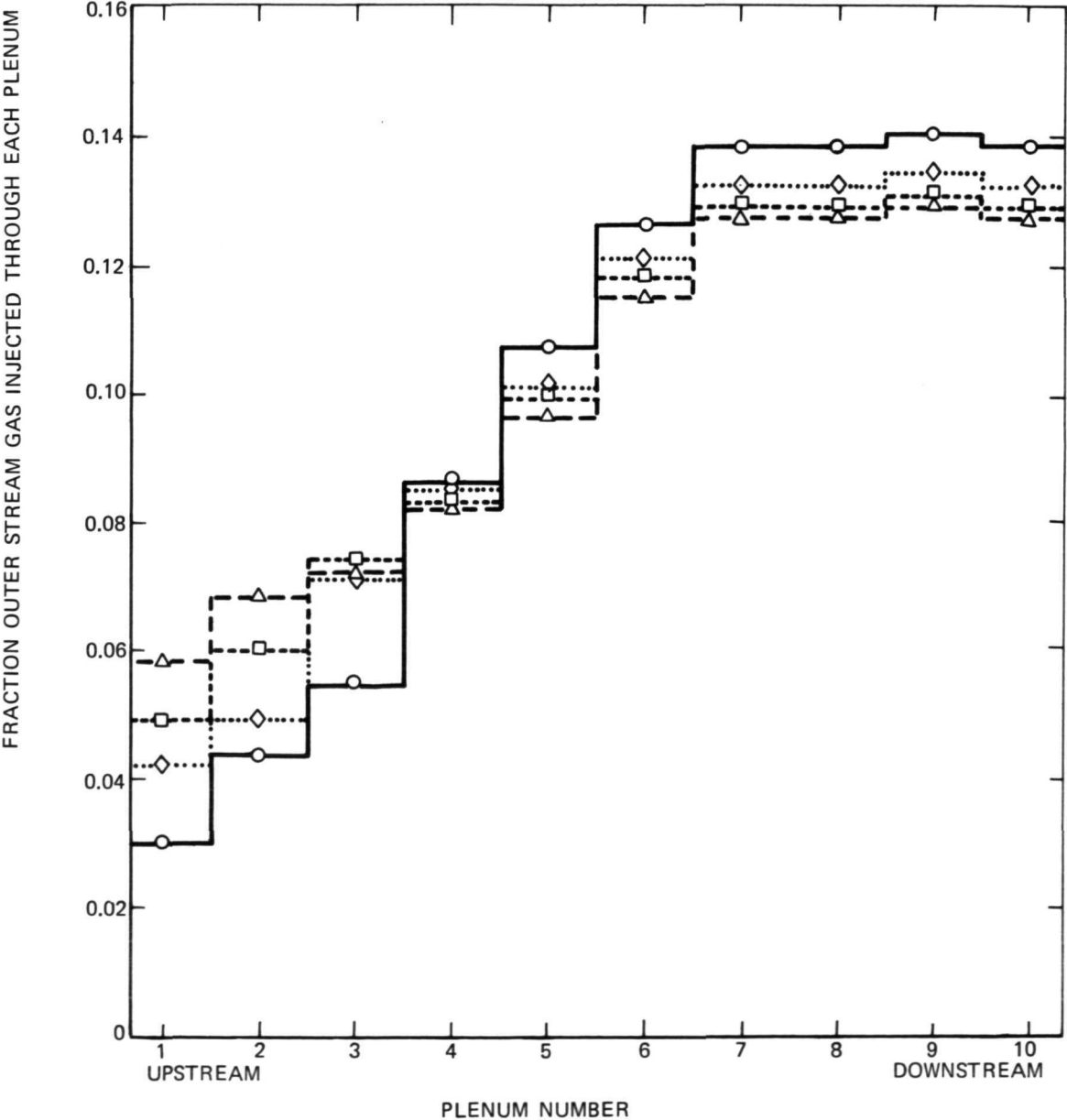
FIGURE 29

FLOW VISULIZATION RESULTS FOR SPHERICAL CAVITY VB

$W_O = 0.5$ lb/sec   (0.23 Kg/sec)
IODINE ADDED TO INNER GAS AS TRACE MATERIAL

OUTER–STREAM FLOW DISTRIBUTION ADJUSTED FOR APPARENT OPTIMUN
CONTAINMENT FOR EACH FLOW CONDITION – SEE FIG. 29

INNER–STREAM
GAS: AIR

INNER–STREAM
GAS: FREON–11

$W_O/W_i \cong$

25

50

100
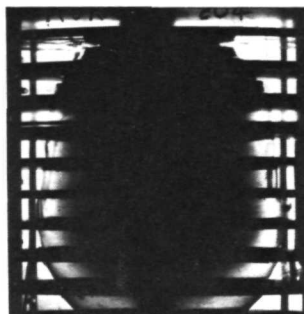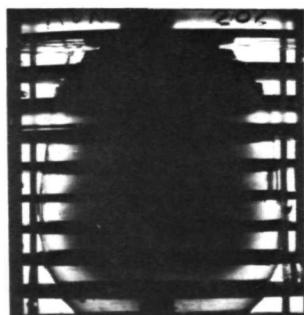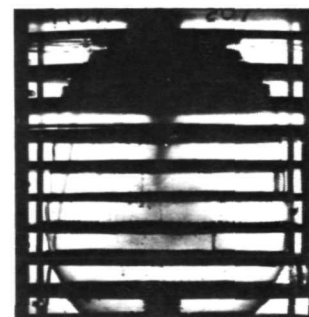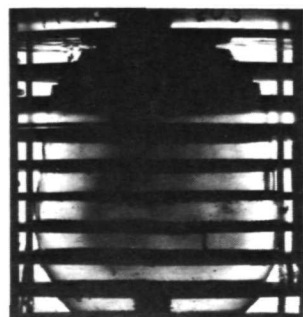
FIGURE 30

60

INNER-GAS CONCENTRATION PROFILES FOR W_o/W_i = 25 AND AIR AS INNER-STREAM GAS

PLENUM NUMBER	2	3	4	5	6	7	8	9	10
SYMBOL	○	□	△	◇	▽	◆	●	■	▲
AXIAL DISTANCE FROM INNER-STREAM INJECTOR	– 1.5	0	+ 1.5	3.0	4.5	6.0	7.5	9.0	10.5

DOWNSTREAM SECTION

UPSTREAM SECTION
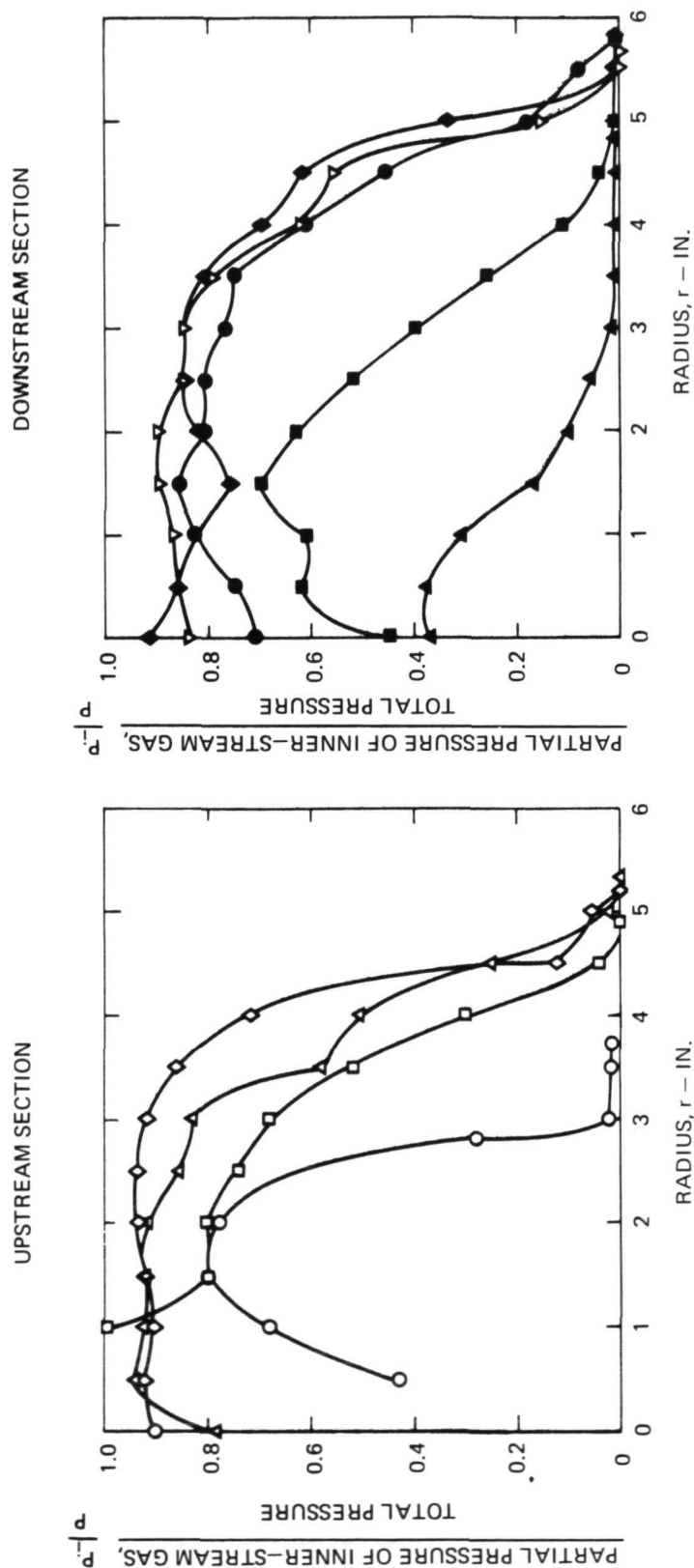
FIGURE 31

61

INNER–GAS CONCENTRATION PROFILES FOR W_o/W_i = 50 AND AIR AS INNER–STREAM GAS

PLENUM NUMBER	2	3	4	5	6	7	8	9	10
SYMBOL	○	□	△	◇	▽	◆	●	■	▲
AXIAL DISTANCE FROM INNER–STREAM INJECTOR	– 1.5	0	+ 1.5	3.0	4.5	6.0	7.5	9.0	10.5
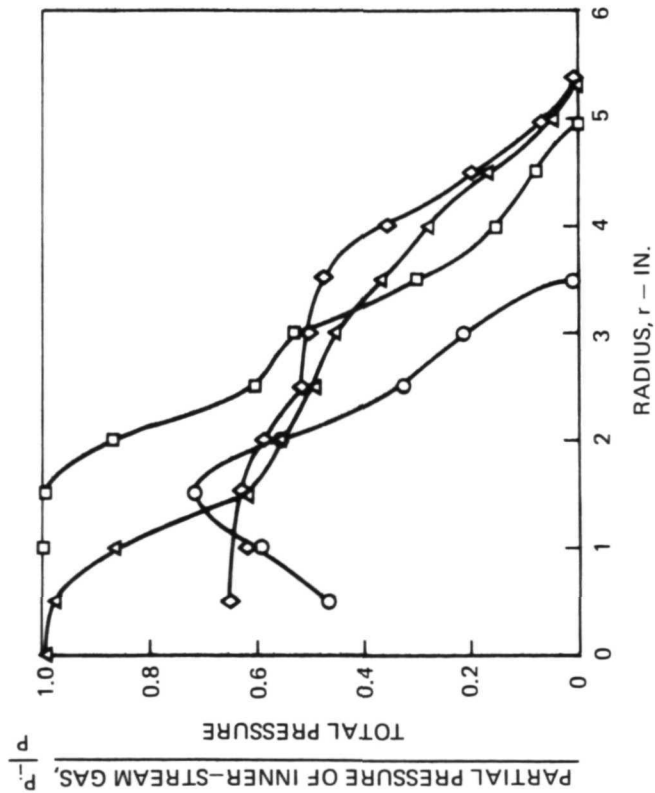
DOWNSTREAM SECTION

UPSTREAM SECTION
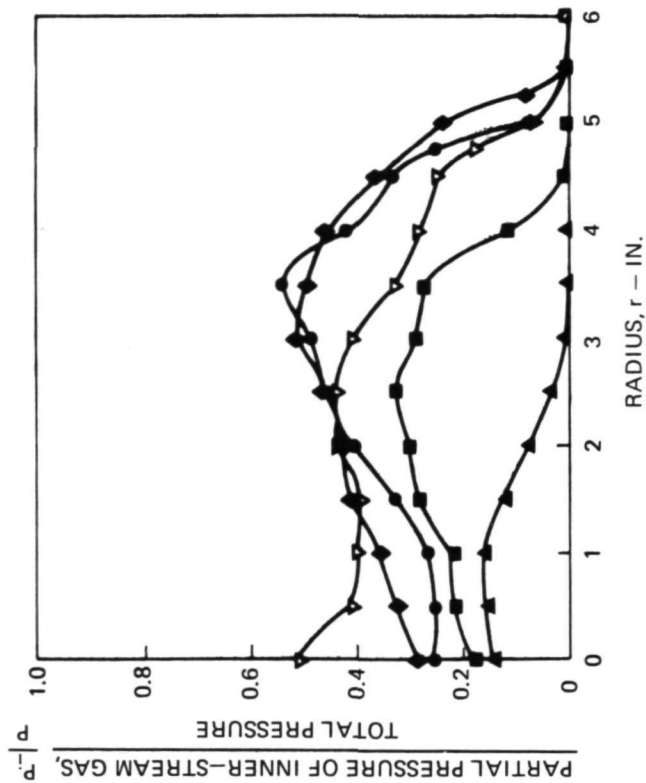
FIGURE 32

62

INNER–GAS CONCENTRATION PROFILES FOR W_o/W_i = 100 AND AIR AS INNER–STREAM GAS

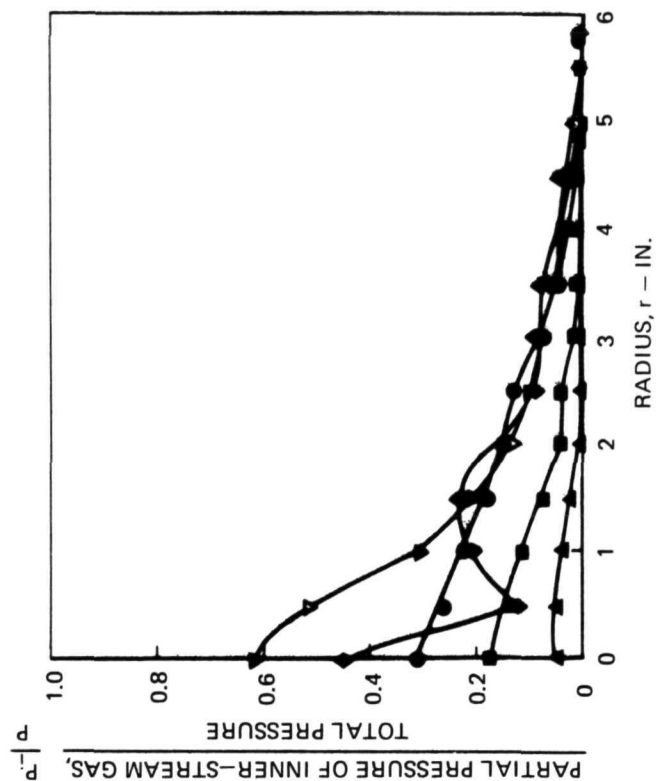| PLENUM NUMBER	2	3	4	5	6	7	8	9	10
SYMBOL	○	□	△	◇	▽	◆	●	■	▲
AXIAL DISTANCE FROM INNER–STREAM INJECTOR	– 1.5	0	+ 1.5	3.0	4.5	6.0	7.5	9.0	10.5
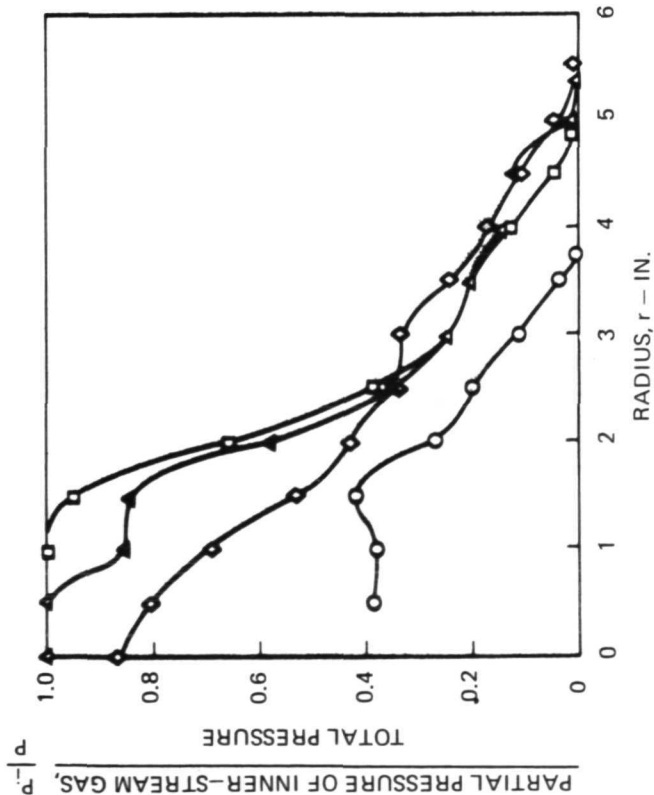
DOWNSTREAM SECTION

UPSTREAM SECTION
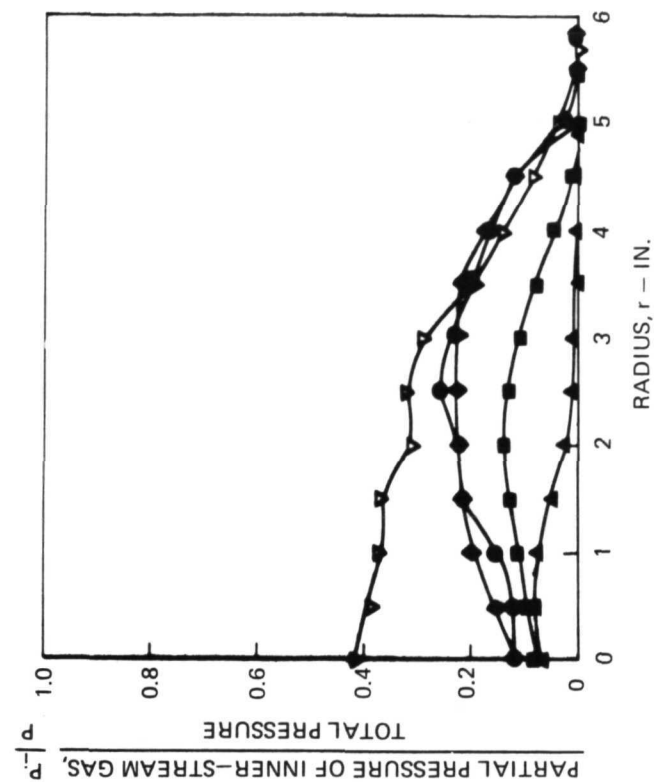
FIGURE 33

63

INNER–GAS CONCENTRATION PROFILES FOR W_o/W_i = 25 AND FREON 11 AS INNER–STREAM GAS

BUOYANCY NUMBER, B = 7

PLENUM NUMBER	2	3	4	5	6	7	8	9	10
SYMBOL	○	□	△	◇	▽	◆	●	■	▲
AXIAL DISTANCE FROM INNER–STREAM INJECTOR	– 1.5	0	+ 1.5	3.0	4.5	6.0	7.5	9.0	10.5
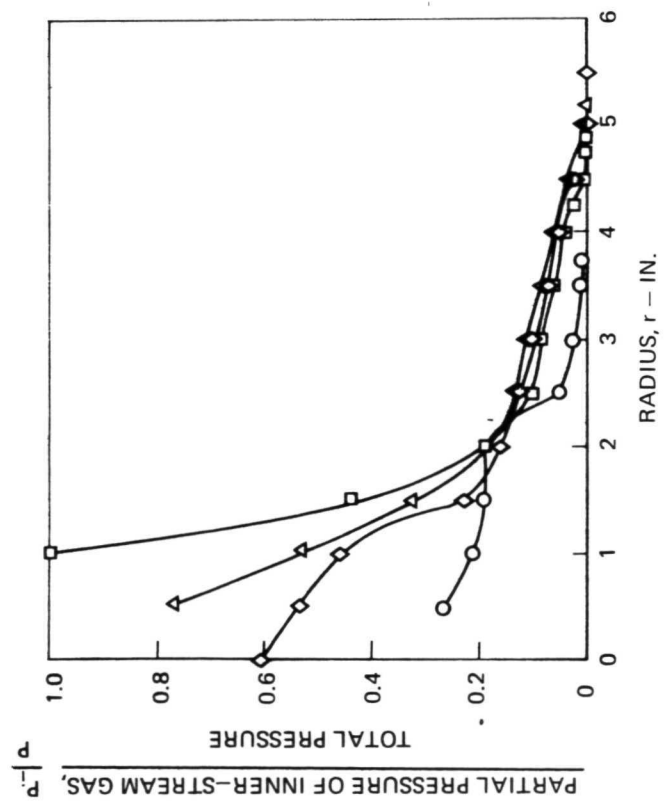
DOWNSTREAM SECTION

UPSTREAM SECTION
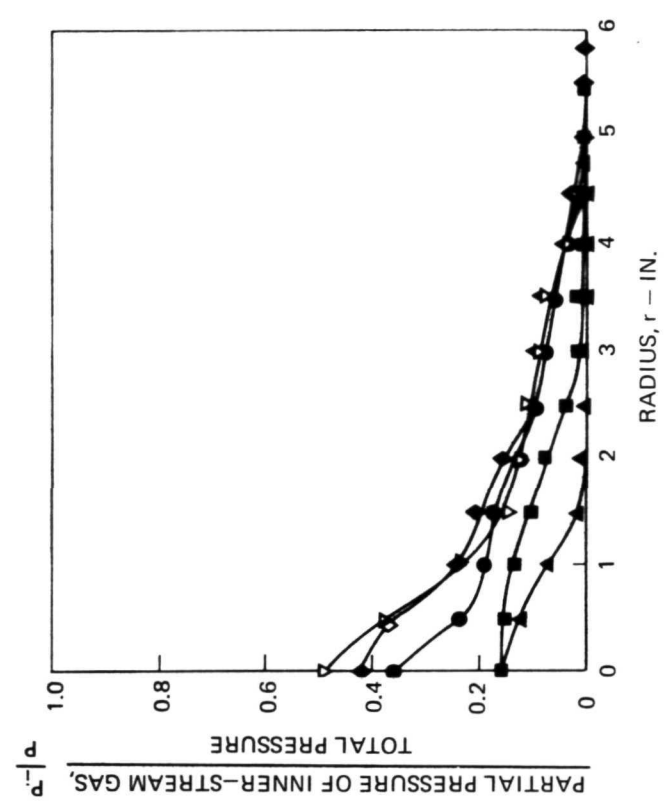
FIGURE 34

64

INNER–GAS CONCENTRATION PROFILES FOR $W_o/W_i = 50$ AND FREON 11 AS INNER–STREAM GAS

BUOYANCY NUMBER, B = 15

PLENUM NUMBER	2	3	4	5	6	7	8	9	10
SYMBOL	○	□	△	◇	▽	◆	●	■	▲
AXIAL DISTANCE FROM INNER–STREAM INJECTOR	– 1.5	0	+ 1.5	3.0	4.5	6.0	7.5	9.0	10.5
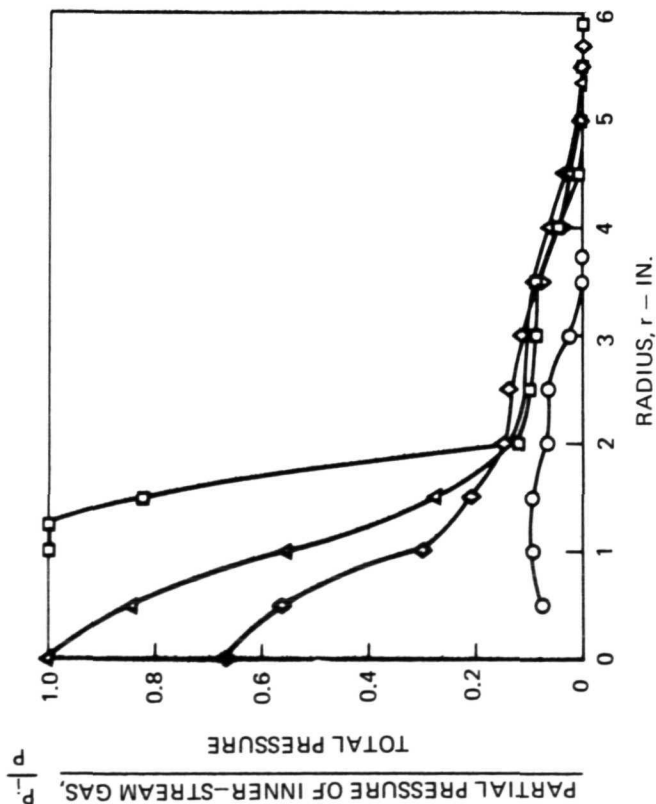
DOWNSTREAM SECTION

UPSTREAM SECTION

FIGURE 35

65

INNER–GAS CONCENTRATION PROFILES FOR W_o/W_i = 100 AND FREON 11 AS INNER–STREAM GAS

BUOYANCY NUMBER, B = 30

PLENUM NUMBER	2	3	4	5	6	7	8	9	10
SYMBOL	○	□	△	◇	▽	◆	●	■	▲
AXIAL DISTANCE FROM INNER–STREAM INJECTOR	– 1.5	0	+ 1.5	3.0	4.5	6.0	7.5	9.0	10.5
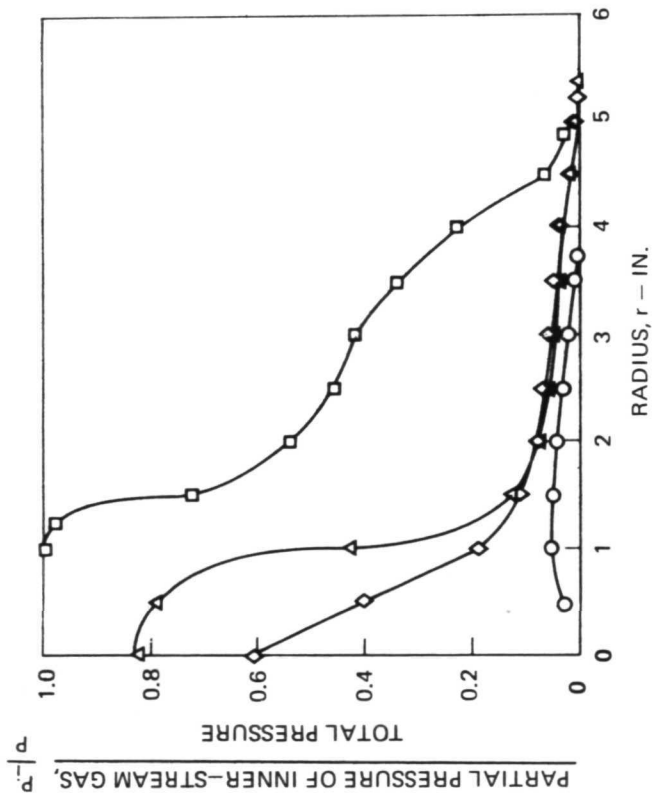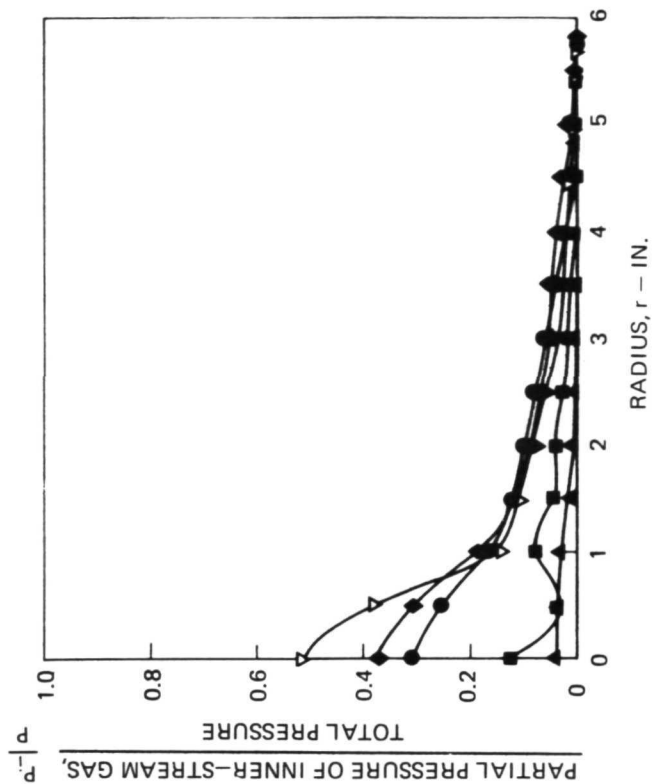
FIGURE 36

AXIAL DISTRIBUTION OF INTEGRAL RESULTS AND CAVITY—AVERAGED
RESULTS FROM INNER— GAS CONCENTRATION MEASUREMENTS

SYMBOL	RUN No.	W_o/W_i	$\bar{P}_i/P$	INNER—GAS
●	204	25	0.40	AIR
■	202	50	0.27	AIR
▲	203	100	0.15	AIR
○	205	25	0.07	FREON 11
□	206	50	0.07	FREON 11
△	207	100	0.07	FREON 11
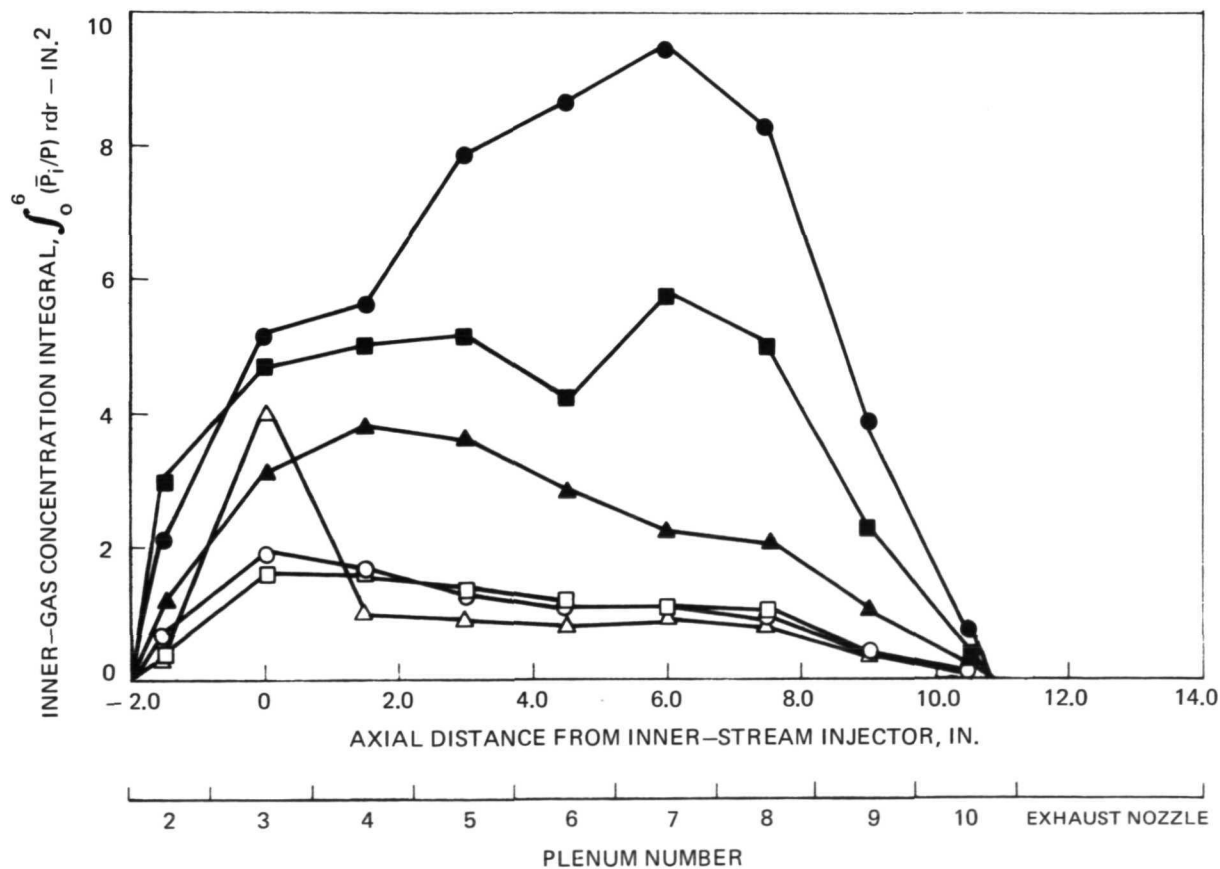
FIGURE 37

67

COMPARISON OF CALCULATED AND MEASURED
INNER–STREAM CONCENTRATION PROFILES

PARAMETER	W_o lb/sec	W_i lb/sec	INNER GAS	OUTER–STREAM INJECTION DISTRIBUTION	CAVITY SHAPE	KINEMATIC VISCOSITY, ν – ft^2/sec	GRAVITY FIELD	$\overline{P}_i/P$
ANALYSIS	0.5	0.01	FREON–11	CASE IV TABLE III	I FIG. 4	0.1	1 "g" TOWARD NOZZLE	0.04
EXPERIMENT	0.5	0.01	FREON–11	RUN 206 FIG. 29	VB FIG. 26	UNKNOWN	1 "g" TOWARD NOZZLE	0.06

SYMBOL BOX

PLENUM NUMBER	2	3	4	5	6	7	8	9
ANALYTICAL	◐	◧	▲	◆	▼	◈	◑	◨
EXPERIMENTAL	○	□	△	◇	▽	◆	●	■
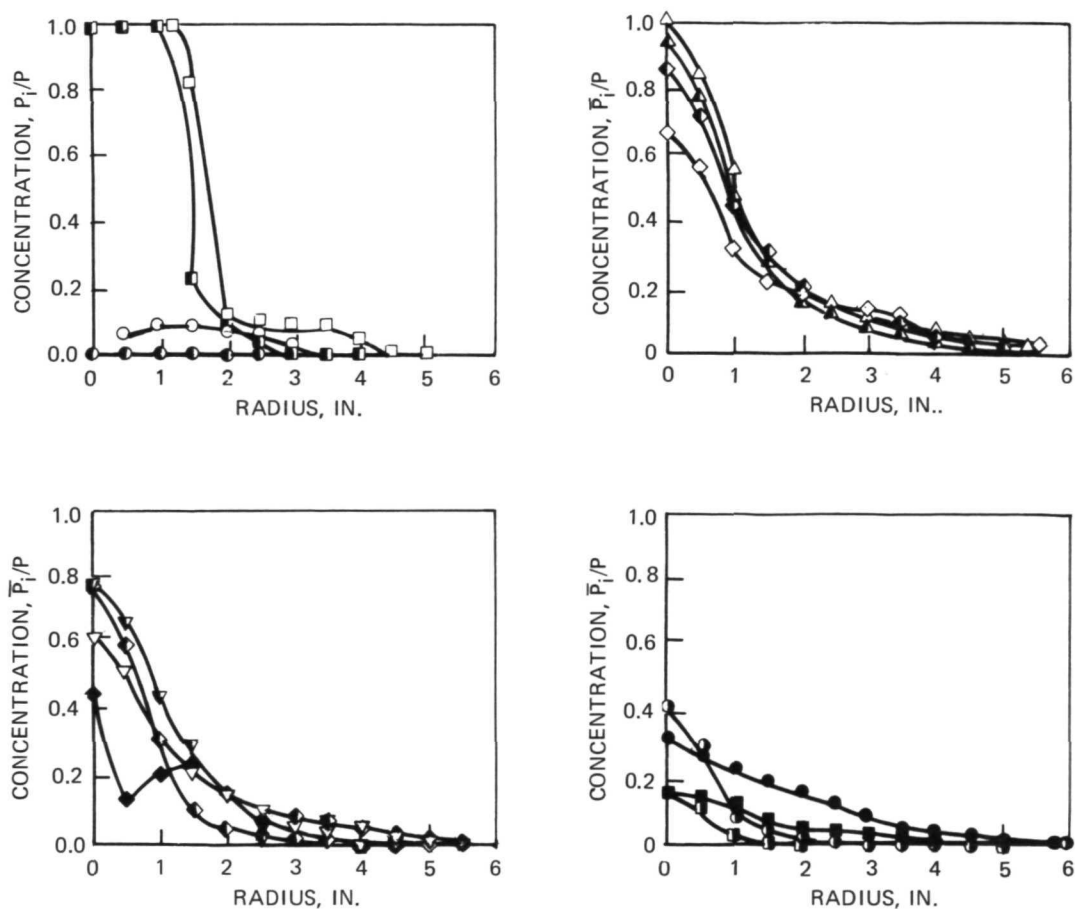
FIGURE 38

68

COMPARISON OF PRESENT SPHERICAL CAVITY AND PREVIOUS COAXIAL FLOW
CONTAINMENT RESULTS WITH GNR OPEN–CYCLE FLUID MECHANICS REQUIREMENTS

BEST CONTAINMENT RESULTS FROM EACH SOURCE USED IN COMPARISON

SYMBOL	INNER GAS	$\bar{P}_i/P_0$	CAVITY SHAPE	SOURCE	MEASUREMENT TECHNIQUES
△-----△	AIR	1.0	'SPHERICAL' – COMBINATION WALL JET	PRESENT WORK	MASS SPECTROMETER
▲-----▲	FREON–11	4.7			
○——○	AIR	1.0	CYLINDRICAL – FOAM INLET COAXIAL FLOW	REF. 10	CHORDAL LIGHT ABSORPTOMETER
●——●	FREON–11	4.7			
□—·—□	AIR	1.0	CYLINDRICAL – SCREEN INLET COAXIAL FLOW	REF. 4	
■—·—■	FREON–11	4.7			
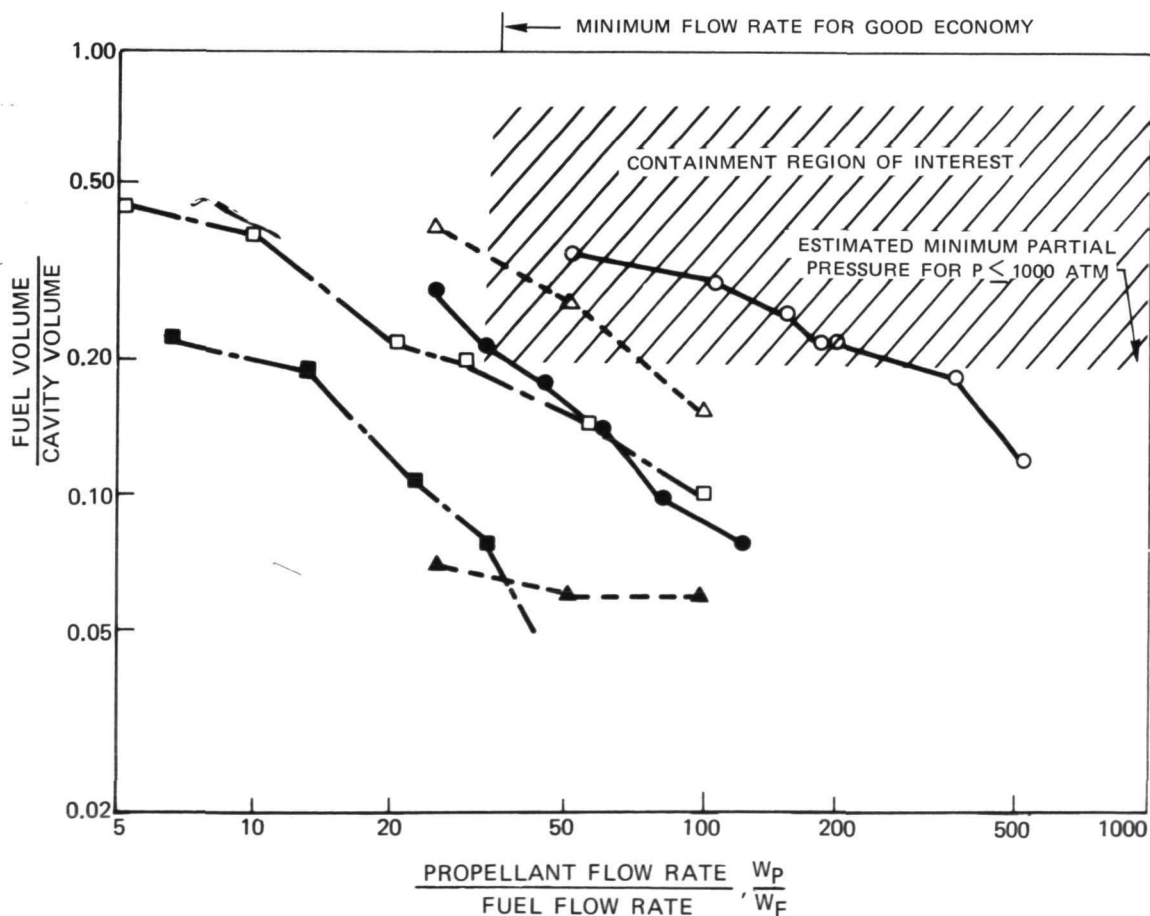
FIGURE 39

"The aeronautical and space activities of the United States shall be conducted so as to contribute . . . to the expansion of human knowledge of phenomena in the atmosphere and space. The Administration shall provide for the widest practicable and appropriate dissemination of information concerning its activities and the results thereof."

—NATIONAL AERONAUTICS AND SPACE ACT OF 1958

NASA SCIENTIFIC AND TECHNICAL PUBLICATIONS

TECHNICAL REPORTS: Scientific and technical information considered important, complete, and a lasting contribution to existing knowledge.

TECHNICAL NOTES: Information less broad in scope but nevertheless of importance as a contribution to existing knowledge.

TECHNICAL MEMORANDUMS: Information receiving limited distribution because of preliminary data, security classification, or other reasons. Also includes conference proceedings with either limited or unlimited distribution.

CONTRACTOR REPORTS: Scientific and technical information generated under a NASA contract or grant and considered an important contribution to existing knowledge.

TECHNICAL TRANSLATIONS: Information published in a foreign language considered to merit NASA distribution in English.

SPECIAL PUBLICATIONS: Information derived from or of value to NASA activities. Publications include final reports of major projects, monographs, data compilations, handbooks, sourcebooks, and special bibliographies.

TECHNOLOGY UTILIZATION PUBLICATIONS: Information on technology used by NASA that may be of particular interest in commercial and other non-aerospace applications. Publications include Tech Briefs, Technology Utilization Reports and Technology Surveys.

Details on the availability of these publications may be obtained from:

SCIENTIFIC AND TECHNICAL INFORMATION OFFICE

NATIONAL AERONAUTICS AND SPACE ADMINISTRATION

Washington, D.C. 20546